Chapter 7
Tool Point Dynamics Prediction

The secret to creativity is knowing how to hide your sources.

- Albert Einstein

In Chapters 4, 5, and 6 we analyzed several aspects of milling with the ultimate goal of enabling *a priori* stability and surface location error predictions in order to improve productivity. We described frequency-domain solutions that offer closed form expressions for both stability (Chapter 4) and surface location error (Chapter 5). The primary inputs to these analyses are the force model coefficients and tool point frequency response function, or FRF. In this chapter, we apply the receptance coupling technique to prediction of the tool point response in order to complement the frequency-domain process models detailed previously.[1] We also include a brief review of Euler-Bernoulli beam theory and provide closed form solutions for the direct and cross receptances (FRFs) under free-free and clamped-free boundary conditions.

7.1 Motivation

While impact testing (Section 2.6) provides a convenient approach to obtaining the tool-holder-spindle-machine[2] FRF (typically measured at the tool point), it requires a separate set of measurements for each assembly. For example, if there are 25 tools in a machine tool's magazine, then a minimum of 50 measurements are required (one each for the x and y directions, assuming the axial compliance in the z direction is negligible). Further, if the tool insertion length is modified due to new requirements or inadequate control during tooling setup, the measurements must be repeated for that tool-holder combination. This requirement

[1] If the tool point FRF is known, the modal fitting procedure described in Section 2.5 can be applied to identify the modal parameters required for time-domain simulation as well.

[2] The workpiece can also be the source of significant dynamic compliance. However, we will limit our discussions to situations where the workpiece can be assumed to be rigid relative to the tool-holder-spindle-machine assembly.

T.L. Schmitz, K.S. Smith, *Machining Dynamics*, DOI 10.1007/978-0-387-09645-2_7,

for multiple measurements certainly does not preclude the application of the process analyses we've discussed in production environments. However, the required time and cost for impact testing does pose an obstacle to convenient implementation at the shop floor level.

IN A NUTSHELL Although FRF measurements provide us with essential information, they are specific to the setup. The tool-holder-spindle-machine FRF changes strongly with tool length and diameter, for example. Unfortunately, modern CNC systems encourage poor setup repeatability by including tool length offset correction. Although this may enable you to put the tool point at the correct geometric location, it also leads to almost certain variability in day to day machining performance due to the change in assembly dynamics.

While no predictive approach replaces actual data, the requirement for a separate measurement of every conceivable setup can lead to a substantial number of measurements. In this chapter we describe a new method that eliminates the need to measure each tool-holder in a particular spindle. By combining measurements of a simple artifact inserted in the spindle in question with models of tools and holders, we can perform off line FRF predictions for a range of tools.

7.2 Basic Receptance Coupling

Rather than consider the tool-holder-spindle-machine combination as a single assembly, we can view it as being composed of three separate entities, specifically, the tool, the holder, and the spindle-machine. Of these three, the tool and holder are convenient to model because they are not structurally complicated. The spindle-machine, on the other hand, is much more challenging. Spindle dynamics modeling, often completed using finite element analysis, requires detailed knowledge of the mechanical design, bearing stiffness values (which depend on the assembly tolerances), and damping levels[3]. For commercial machining centers, the spindle design is often proprietary or unavailable to the end user, and the bearing stiffness values are difficult to obtain. Also, first principle estimates of the spindle damping remains an active research area. Comparable problems are encountered in modeling the machine dynamics, particularly obtaining the damping values, which often depend on multiple energy dissipation mechanisms and locations. Even more problematic, different lengths and diameters of tools may activate these mechanisms by differing amounts (especially within the spindle).

[3] Author T. Schmitz acknowledges conversations with N. Arakere, University of Florida, regarding dynamic modeling of rotating systems.

FOR INSTANCE A short, large diameter tool may be very stiff and emphasize the spindle modes in the assembly FRF. The primary damping source in this case would be the spindle bearings and interface between the spindle and motor rotor. If the tool is long and slender, by contrast, the spindle may appear nearly rigid (but not always![4]). This tool geometry would generally emphasize the damping in the tool-tool holder-spindle interfaces with relatively less energy dissipated by the spindle bearings.

This leads us to a scenario where we can consider modeling those components that lend themselves to this activity (the tool and holder) and measuring the difficult-to-model element (the spindle-machine)[5]. Additionally, rather than describing the modeled and measured parts, or substructures, using modal parameters, for example, it is sensible to develop substructure FRFs since the assembly FRF is a primary input for the analytical milling process analyses. A convenient approach for joining these substructure FRFs to obtain the assembly response is receptance coupling [1, 2], or receptance coupling substructure analysis (RCSA) as referenced in recent literature [3–12]. Prior to detailing RCSA for tool point FRF prediction, let's examine receptance coupling solutions for some simple dynamic systems.

7.2.1 Two Component Rigid Coupling

As shown in Fig. 7.2.1, two components, I and II, are to be rigidly coupled to form assembly III. The coupling coordinates are x_{1a} and x_{1b} for the two

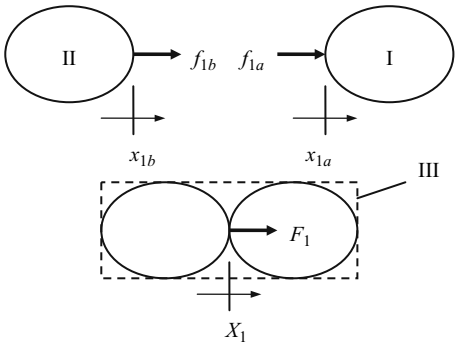

Fig. 7.2.1 Rigid coupling of components I and II to form assembly III. The force F_1 is applied to the assembly in order to determine H_{11}

[4] See Example 7.5.2.

[5] Author T. Schmitz recognizes "hallway" discussions with Dr. J. Pratt, National Institute of Standards and Technology, Gaithersburg, MD, in forming this observation.

substructures I and II, respectively. The corresponding assembly coordinate, X_1, is located at the same physical location as x_{1a} and x_{1b} after they are joined. An attractive aspect of receptance coupling is that the component FRFs are only required at the coupling locations and any point where the assembly response is to be predicted [13–15]. Therefore, the direct (see Section 2.4) assembly response, $H_{11}(\omega) = \frac{X_1}{F_1}$, due to a harmonic force applied at coordinate X_1 can be fully described using the direct component receptances $h_{1a1a}(\omega) = \frac{x_{1a}}{f_{1a}}$ and $h_{1b1b}(\omega) = \frac{x_{1b}}{f_{1b}}$ obtained from harmonic forces applied at x_{1a} and x_{1b}, respectively. Note that we've used upper case variables to designate assembly terms and lower case variables to identify component terms.

To determine the assembly response, we must first state the compatibility condition, $x_{1b} - x_{1a} = 0$, which represents the rigid coupling between component coordinates x_{1a} and x_{1b}. We can therefore write $x_{1b} = x_{1a} = X_1$ due to our decision to locate assembly coordinate X_1 at the (rigid) coupling point. We must also define the equilibrium condition, $f_{1a} + f_{1b} = F_1$, which equates the internal (component) and external (assembly) forces. Let's substitute for the displacements in the compatibility equation.

$$x_{1b} - x_{1a} = 0$$
$$h_{1b1b}f_{1b} - h_{1a1a}f_{1a} = 0$$

We next use the equilibrium condition, rewritten as $f_{1a} = F_1 - f_{1b}$, to eliminate f_{1a}. Rearranging enables us to solve for f_{1b}.

$$h_{1b1b}f_{1b} - h_{1a1a}F_1 + h_{1a1a}f_{1b} = 0$$
$$(h_{1a1a} + h_{1b1b})f_{1b} = h_{1a1a}F_1$$
$$f_{1b} = (h_{1a1a} + h_{1b1b})^{-1}h_{1a1a}F_1$$

Now that we have f_{1b}, we can again use the equilibrium condition to determine f_{1a}.

$$f_{1a} = F_1 - f_{1b}$$
$$f_{1a} = \left(1 - (h_{1a1a} + h_{1b1b})^{-1}h_{1a1a}\right)F_1$$

We solve for H_{11} as shown in Eq. 7.2.1. This equation gives the direct assembly response at the coupling coordinate, X_1, as a function of the component receptances. These frequency dependent, complex valued receptances may have any number of modes. There are no restrictions on the relationship between the number of modes and coordinates as with modal analysis (i.e., we saw in Section 2.4 that the number of modeled modes and coordinates must be equal to obtain square matrices when using modal techniques).

$$H_{11} = \frac{X_1}{F_1} = \frac{x_{1a}}{F_1} = \frac{h_{1a1a} f_{1a}}{F_1} = h_{1a1a} - h_{1a1a}(h_{1a1a} + h_{1b1b})^{-1} h_{1a1a} \qquad (7.2.1)$$

IN A NUTSHELL The spindle-machine FRF, which is difficult to model, is determined by measurement. As we've discussed, the FRF shows the real and imaginary parts of the frequency dependent motion at a selected coordinate in response to a force. The tool and holder, on the other hand, are modeled using beam theory. The measured and modeled FRFs are connected at the appropriate coordinate; this is the essence of receptance coupling. Using this approach, the FRF of the assembled structure can be predicted at any coordinate on the modeled portion of the assembly.

Similarly, we can predict the assembly response at another coordinate, not coincident with the coupling point, by defining the component receptance at the desired location. Consider Fig. 7.2.2, where the direct assembly response at X_1 is again desired, but this location is now at another point on component I. We again assume x_1 and X_1 are collocated before and after coupling. The new coupling coordinates at the rigid coupling point are x_{2a} and x_{2b}. The component receptances corresponding to Fig. 7.2.2 are $h_{11} = \frac{x_1}{f_1}$ and $h_{2a2a} = \frac{x_{2a}}{f_{2a}}$ for I, and $h_{2b2b} = \frac{x_{2b}}{f_{2b}}$ for II. The compatibility condition for the rigid coupling is $x_{2b} - x_{2a} = 0$ and we can therefore write $x_{2a} = x_{2b} = X_2$. Also, $x_1 = X_1$. The equilibrium conditions are $f_{2a} + f_{2b} = 0$ and $f_1 = F_1$.

To determine $H_{11} = \frac{X_1}{F_1}$, we'll first write the component displacements. For I, we now have two forces acting on the body, so the displacements are:

$$x_1 = h_{11} f_1 + h_{12a} f_{2a} \quad \text{and} \quad x_{2a} = h_{2a1} f_1 + h_{2a2a} f_{2a} \qquad (7.2.2)$$

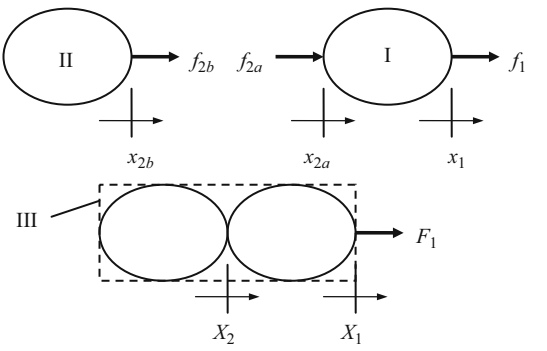

Fig. 7.2.2 Example showing rigid coupling of components I and II to form assembly III. The force F_1 is applied to the assembly in order to determine H_{11} and H_{21}

For II, we have $x_{2b} = h_{2b2b} f_{2b}$. Substitution into the compatibility condition gives:

$$h_{2b2b} f_{2b} - h_{2a1} f_1 - h_{2a2a} f_{2a} = 0. \tag{7.2.3}$$

We apply the equilibrium conditions to replace f_1 and eliminate f_{2a} ($f_{2a} = -f_{2b}$).

$$h_{2b2b} f_{2b} - h_{2a1} F_1 + h_{2a2a} f_{2b} = 0. \tag{7.2.4}$$

This enables us to group terms and solve for f_{2b}. Specifically, we have that $f_{2b} = (h_{2a2a} + h_{2b2b})^{-1} h_{2a1} F_1$. Therefore, we can also write $f_{2a} = -(h_{2a2a} + h_{2b2b})^{-1} h_{2a1} F_1$. Substitution of this force value into the H_{11} expression gives us the desired result; see Eq. 7.2.5. Again, the assembly response is written as a function of the component direct (h_{11}, h_{2a2a}, and h_{2b2b}) and cross (h_{12a} and h_{2a1}) receptances.

$$\begin{aligned} H_{11} &= \frac{X_1}{F_1} = \frac{x_1}{F_1} = \frac{h_{11} f_1 + h_{12a} f_{2a}}{F_1} = \frac{h_{11} f_1 - h_{12a} (h_{2a2a} + h_{2b2b})^{-1} h_{2a1} F_1}{F_1} \\ H_{11} &= \frac{h_{11} F_1 - h_{12a} (h_{2a2a} + h_{2b2b})^{-1} h_{2a1} F_1}{F_1} = h_{11} - h_{12a} (h_{2a2a} + h_{2b2b})^{-1} h_{2a1} \end{aligned} \tag{7.2.5}$$

We can also use f_{2a} to determine the cross receptance H_{21}. See Eq. 7.2.6.

$$\begin{aligned} H_{21} &= \frac{X_2}{F_1} = \frac{x_{2a}}{F_1} = \frac{h_{2a1} f_1 + h_{2a2a} f_{2a}}{F_1} = \frac{h_{2a1} f_1 - h_{2a2a} (h_{2a2a} + h_{2b2b})^{-1} h_{2a1} F_1}{F_1} \\ H_{21} &= \frac{h_{2a1} F_1 - h_{2a2a} (h_{2a2a} + h_{2b2b})^{-1} h_{2a1} F_1}{F_1} = h_{2a1} - h_{2a2a} (h_{2a2a} + h_{2b2b})^{-1} h_{2a1} \end{aligned} \tag{7.2.6}$$

In an analogous way, we can find the direct and cross receptances, H_{22} and H_{12}, respectively, due to a force applied at X_2. See Fig. 7.2.3. The component

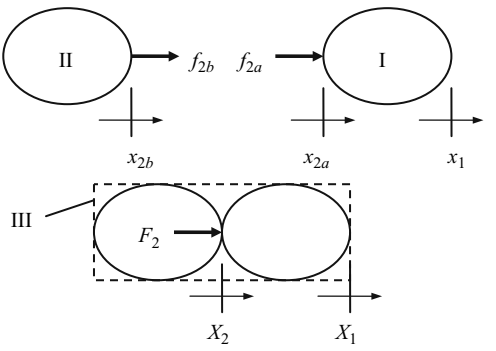

Fig. 7.2.3 Example showing rigid coupling of components I and II to form assembly III. The force F_2 is applied to the assembly in order to determine H_{22} and H_{12}

receptances are again $h_{11} = \frac{x_1}{f_1}$ and $h_{2a2a} = \frac{x_{2a}}{f_{2a}}$ for I, and $h_{2b2b} = \frac{x_{2b}}{f_{2b}}$ for II. The compatibility condition for the rigid coupling remains as $x_{2b} - x_{2a} = 0$. However, the equilibrium condition is $f_{2a} + f_{2b} = F_2$.

To determine $H_{22} = \frac{X_2}{F_2}$, we begin by writing the component displacements. For I, the displacements are:

$$x_1 = h_{12a} f_{2a} \quad \text{and} \quad x_{2a} = h_{2a2a} f_{2a}. \tag{7.2.7}$$

For II, we have $x_{2b} = h_{2b2b} f_{2b}$. Substitution in the compatibility condition gives:

$$h_{2b2b} f_{2b} - h_{2a2a} f_{2a} = 0. \tag{7.2.8}$$

We apply the equilibrium condition, $f_{2a} = F_2 - f_{2b}$, to eliminate f_{2a} in Eq. 7.2.8.

$$h_{2b2b} f_{2b} - h_{2a2a} F_2 + h_{2a2a} f_{2b} = 0 \tag{7.2.9}$$

This enables us to group terms and solve for f_{2b}. We find that $f_{2b} = (h_{2a2a} + h_{2b2b})^{-1} h_{2a2a} F_2$. Again using the equilibrium condition, we can write $f_{2a} = \left(1 - (h_{2a2a} + h_{2b2b})^{-1} h_{2a2a}\right) F_2$. Equation 7.2.10 gives the desired H_{22} expression.

$$\begin{aligned} H_{22} &= \frac{X_2}{F_2} = \frac{x_{2a}}{F_2} = \frac{h_{2a2a} f_{2a}}{F_2} = \frac{h_{2a2a}\left(1 - (h_{2a2a} + h_{2b2b})^{-1} h_{2a2a}\right) F_2}{F_2} \\ H_{22} &= \frac{h_{2a2a} F_2 - h_{2a2a}(h_{2a2a} + h_{2b2b})^{-1} h_{2a2a} F_2}{F_2} = h_{2a2a} - h_{2a2a}(h_{2a2a} + h_{2b2b})^{-1} h_{2a2a} \end{aligned} \tag{7.2.10}$$

We use f_{2a} to find the cross receptance H_{12} as well. See Eq. 7.2.11.

$$\begin{aligned} H_{12} &= \frac{X_1}{F_2} = \frac{x_1}{F_2} = \frac{h_{12a} f_{2a}}{F_2} = \frac{h_{12a}\left(1 - (h_{2a2a} + h_{2b2b})^{-1} h_{2a2a}\right) F_2}{F_2} \\ H_{12} &= h_{12a} - h_{12a}(h_{2a2a} + h_{2b2b})^{-1} h_{2a2a} \end{aligned} \tag{7.2.11}$$

7.2.2 Two Component Flexible Coupling

Let's continue with the system shown in Fig. 7.2.1, but now couple the two components through a linear spring, described by the constant k. This is displayed in Fig. 7.2.4. The component receptances are $h_{1a1a} = \frac{x_{1a}}{f_{1a}}$ and $h_{1b1b} = \frac{x_{1b}}{f_{1b}}$ and the equilibrium condition is $f_{1a} + f_{1b} = F_{1a}$. These are analogous to the rigid coupling case. However, the compatibility condition now becomes:

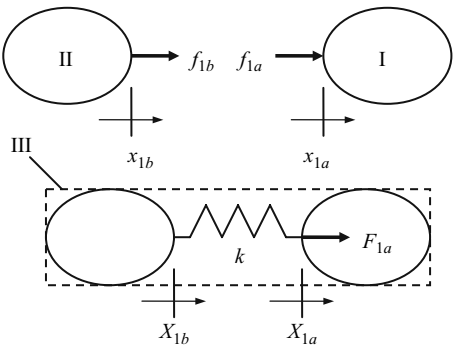

Fig. 7.2.4 Flexible coupling of components I and II to form assembly III. The force F_{1a} is applied to the assembly in order to determine H_{1a1a} and H_{1b1a}

$$k(x_{1b} - x_{1a}) = -f_{1b}. \tag{7.2.12}$$

Because the component and assembly coordinates are coincident, we have that $x_{2a} = X_{2a}$ and $x_{2b} = X_{2b}$. To determine $H_{1a1a} = \frac{X_{1a}}{F_{1a}}$, let's first substitute the component displacements in the compatibility condition. See Eq. 7.2.13.

$$k(h_{1b1b}f_{1b} - h_{1a1a}f_{1a}) = -f_{1b} \tag{7.2.13}$$

Using the equilibrium condition, $f_{1a} = F_{1a} - f_{1b}$, we can eliminate f_{1a} to obtain the equation for f_{1b}.

$$\begin{aligned}
&k(h_{1b1b}f_{1b} - h_{1a1a}F_{1a} + h_{1a1a}f_{1b}) = -f_{1b}\\
&kh_{1b1b}f_{1b} - kh_{1a1a}F_{1a} + kh_{1a1a}f_{1b} = -f_{1b}\\
&\left(h_{1a1a} + h_{1b1b} + \frac{1}{k}\right)f_{1b} = h_{1a1a}F_{1a}\\
&f_{1b} = \left(h_{1a1a} + h_{1b1b} + \frac{1}{k}\right)^{-1} h_{1a1a}F_{1a}
\end{aligned}$$

Using f_{1b} and the equilibrium condition, we find that $f_{1a} = \left(1 - \left(h_{1a1a} + h_{1b1b} + \frac{1}{k}\right)^{-1} h_{1a1a}\right)F_{1a}$. Substitution then yields the direct assembly receptance H_{1a1a} as shown in Eq. 7.2.14. We can see that this equation simplifies to Eq. 7.2.1 as k approaches infinity (rigid connection).

$$\begin{aligned}
H_{1a1a} &= \frac{X_{1a}}{F_{1a}} = \frac{x_{1a}}{F_{1a}} = \frac{h_{1a1a}f_{1a}}{F_{1a}} = \frac{h_{1a1a}\left(1 - \left(h_{1a1a} + h_{1b1b} + \frac{1}{k}\right)^{-1} h_{1a1a}\right)F_{1a}}{F_{1a}}\\
H_{1a1a} &= h_{1a1a} - h_{1a1a}\left(h_{1a1a} + h_{1b1b} + \frac{1}{k}\right)^{-1} h_{1a1a}
\end{aligned} \tag{7.2.14}$$

The cross receptance due to the force F_{1a} is provided in Eq. 7.2.15.

$$H_{1b1a} = \frac{X_{1b}}{F_{1a}} = \frac{x_{1b}}{F_{1a}} = \frac{h_{1b1b}f_{1b}}{F_{1a}} = \frac{h_{1b1b}\left(h_{1a1a} + h_{1b1b} + \frac{1}{k}\right)^{-1}h_{1a1a}F_{1a}}{F_{1a}}$$
$$H_{1b1a} = h_{1b1b}\left(h_{1a1a} + h_{1b1b} + \frac{1}{k}\right)^{-1}h_{1a1a} \tag{7.2.15}$$

As shown in Fig. 7.2.5, we can alternately apply the assembly force to coordinate X_{1b}. The component receptances and displacements are unchanged, but the equilibrium condition is $f_{1a} + f_{1b} = F_{1b}$. Similarly, we modify the compatibility condition to be:

$$k(x_{1a} - x_{1b}) = -f_{1a}. \tag{7.2.16}$$

Substitution for the component displacements and f_{1b} (from the equilibrium condition) yields the expression for f_{1a}.

$$k(h_{1a1a}f_{1a} - h_{1b1b}F_{1b} + h_{1b1b}f_{1a}) = -f_{1a}$$
$$kh_{1a1a}f_{1a} - kh_{1b1b}F_{1b} + kh_{1b1b}f_{1a} = -f_{1a}$$
$$\left(h_{1a1a} + h_{1b1b} + \frac{1}{k}\right)f_{1a} = h_{1b1b}F_{1b}$$
$$f_{1a} = \left(h_{1a1a} + h_{1b1b} + \frac{1}{k}\right)^{-1}h_{1b1b}F_{1b}$$

Again applying the equilibrium condition, $f_{1b} = F_{1b} - f_{1a}$, we obtain $f_{1b} = \left(1 - \left(h_{1a1a} + h_{1b1b} + \frac{1}{k}\right)^{-1}h_{1b1b}\right)F_{1b}$. Substitution then gives the assembly direct and cross receptances due to F_{1b}.

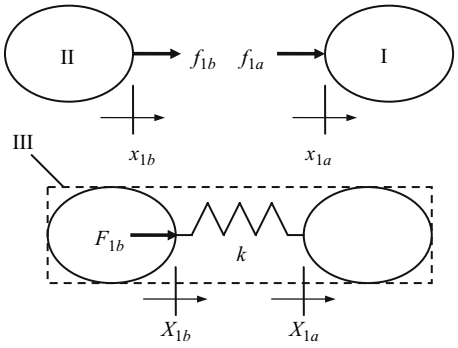

Fig. 7.2.5 Flexible coupling of components I and II to form assembly III. The force F_{1b} is applied to the assembly in order to determine H_{1b1b} and H_{1a1b}

$$H_{1b1b} = \frac{X_{1b}}{F_{1b}} = \frac{x_{1b}}{F_{1b}} = \frac{h_{1b1b}f_{1b}}{F_{1b}} = \frac{h_{1b1b}\left(1 - \left(h_{1a1a} + h_{1b1b} + \frac{1}{k}\right)^{-1} h_{1b1b}\right)F_{1b}}{F_{1b}}$$
$$H_{1b1b} = h_{1b1b} - h_{1b1b}\left(h_{1a1a} + h_{1b1b} + \frac{1}{k}\right)^{-1} h_{1b1b} \tag{7.2.17}$$

$$H_{1a1b} = \frac{X_{1a}}{F_{1b}} = \frac{x_{1a}}{F_{1b}} = \frac{h_{1a1a}f_{1a}}{F_{1b}} = \frac{h_{1a1a}\left(h_{1a1a} + h_{1b1b} + \frac{1}{k}\right)^{-1} h_{1b1b}F_{1b}}{F_{1b}}$$
$$H_{1a1b} = h_{1a1a}\left(h_{1a1a} + h_{1b1b} + \frac{1}{k}\right)^{-1} h_{1b1b} \tag{7.2.18}$$

Similar to the rigid connection example depicted in Fig. 7.2.2, we can again add another coordinate, not located at the coupling location, and apply the external force at that point. See Fig. 7.2.6. The component displacements are again $x_1 = h_{11}f_1 + h_{12a}f_{2a}$ and $x_{2a} = h_{2a1}f_1 + h_{2a2a}f_{2a}$ for substructure I and $x_{2b} = h_{2b2b}f_{2b}$ for substructure II. The equilibrium conditions are $f_{2a} + f_{2b} = 0$ and $f_1 = F_1$. The compatibility condition is:

$$k(x_{2b} - x_{2a}) = -f_{2b}. \tag{7.2.19}$$

As before, the component and assembly coordinates are coincident, so we have that $x_1 = X_1$, $x_{2a} = X_{2a}$, and $x_{2b} = X_{2b}$. To determine $H_{11} = \frac{X_1}{F_1}$, let's first substitute the component displacements in the compatibility condition. See Eq. 7.2.20.

$$k(h_{2b2b}f_{2b} - h_{2a1}f_1 - h_{2a2a}f_{2a}) = -f_{2b} \tag{7.2.20}$$

Using the equilibrium conditions, we can eliminate f_{2a} and replace f_1 with F_1 to obtain the equation for f_{2b}.

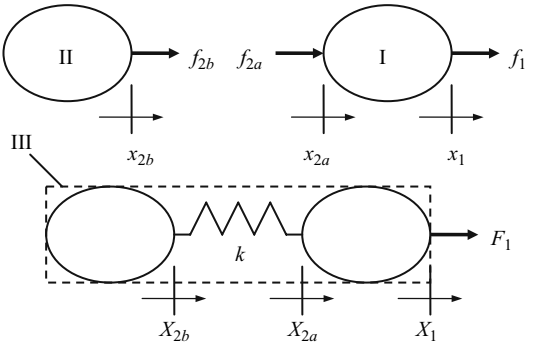

Fig. 7.2.6 Flexible coupling of components I and II to form assembly III. The force F_1 is applied to the assembly in order to determine H_{11}, H_{2a1}, and H_{2b1}

$$k(h_{2b2h}f_{2a} - h_{2a1}F_1 + h_{2a2a}f_{2b}) = -f_{2b}$$
$$kh_{2b2h}f_{2b} - kh_{2a1}F_1 + kh_{2a2a}f_{2b} = -f_{2b}$$
$$\left(h_{2a2a} + h_{2b2b} + \frac{1}{k}\right)f_{2b} = h_{2a1}F_1$$
$$f_{2b} = \left(h_{2a2a} + h_{2b2b} + \frac{1}{k}\right)^{-1} h_{2a1}F_1$$

Applying the equilibrium condition $f_{2a} = -f_{2b}$, we obtain:

$$f_{2a} = -\left(h_{2a2a} + h_{2b2b} + \frac{1}{k}\right)^{-1} h_{2a1}F_1.$$

This enables us to write the direct and cross receptances as shown in Eqs. 7.2.21 and 7.2.22, respectively. We note that these equations simplify to the rigid coupling results provided in Eqs. 7.2.5 and 7.2.6 as k approaches infinity. The assembly cross receptance at coordinate X_{2b} is given by Eq. 7.2.23.

$$H_{11} = \frac{X_1}{F_1} = \frac{x_1}{F_1} = \frac{h_{11}f_1 + h_{12a}f_{2a}}{F_1} = \frac{h_{11}f_1 - h_{12a}\left(h_{2a2a} + h_{2b2b} + \frac{1}{k}\right)^{-1}h_{2a1}F_1}{F_1}$$
$$H_{11} = \frac{h_{11}F_1 - h_{12a}\left(h_{2a2a} + h_{2b2b} + \frac{1}{k}\right)^{-1}h_{2a1}F_1}{F_1} = h_{11} - h_{12a}\left(h_{2a2a} + h_{2b2b} + \frac{1}{k}\right)^{-1} h_{2a1} \tag{7.2.21}$$

$$H_{2a1} = \frac{X_{2a}}{F_1} = \frac{x_{2a}}{F_1} = \frac{h_{2a1}f_1 + h_{2a2a}f_{2a}}{F_1} = \frac{h_{2a1}F_1 - h_{2a2a}\left(h_{2a2a} + h_{2b2b} + \frac{1}{k}\right)^{-1}h_{2a1}F_1}{F_1}$$
$$H_{2a1} = h_{2a1} - h_{2a2a}\left(h_{2a2a} + h_{2b2b} + \frac{1}{k}\right)^{-1} h_{2a1} \tag{7.2.22}$$

$$H_{2b1} = \frac{X_{2b}}{F_1} = \frac{x_{2b}}{F_1} = \frac{h_{2b2h}f_{2b}}{F_1} = \frac{h_{2b2b}\left(h_{2a2a} + h_{2b2b} + \frac{1}{k}\right)^{-1}h_{2a1}F_1}{F_1}$$
$$H_{2b1} = h_{2b2b}\left(h_{2a2a} + h_{2b2b} + \frac{1}{k}\right)^{-1} h_{2a1} \tag{7.2.23}$$

Let's now apply the external force, F_{2a}, to coordinate X_{2a} as shown in Fig. 7.2.7 in order to determine the assembly receptances H_{2a2a}, H_{2b2a}, and H_{12a}. The component displacements are $x_1 = h_{12a}f_{2a}$ and $x_{2a} = h_{2a2a}f_{2a} < ?A3B2tlsb$ for substructure I and $x_{2b} = h_{2b2h}f_{2b}$ for substructure II. The equilibrium condition is $f_{2a} + f_{2b} = F_{2a}$ and the compatibility condition is:

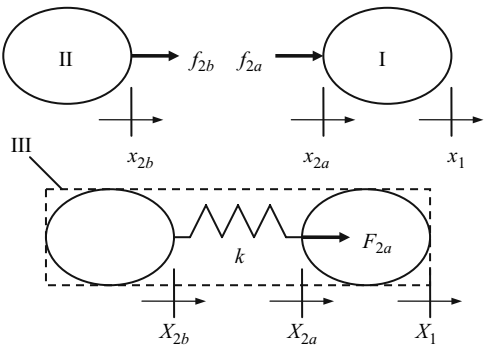

Fig. 7.2.7 Flexible coupling of components I and II to form assembly III. The force F_{2a} is applied to the assembly in order to determine H_{2a2a}, H_{2b2a}, and H_{12a}

$$k(x_{2b} - x_{2a}) = -f_{2b}. \tag{7.2.24}$$

We first determine the force f_{2b} by substituting the component displacements in Eq. 7.2.24 and replacing f_{2a} with $F_{2a} - f_{2b}$.

$$\begin{aligned}
&k(h_{2b2b}f_{2b} - h_{2a2a}F_{2a} + h_{2a2a}f_{2b}) = -f_{2b}\\
&kh_{2b2b}f_{2b} - kh_{2a2a}F_{2a} + kh_{2a2a}f_{2b} = -f_{2b}\\
&\left(h_{2a2a} + h_{2b2b} + \frac{1}{k}\right)f_{2b} = h_{2a2a}F_{2a}\\
&f_{2b} = \left(h_{2a2a} + h_{2b2b} + \frac{1}{k}\right)^{-1} h_{2a2a}F_{2a}
\end{aligned}$$

Again using the equilibrium condition we find the equation for f_{2a}.

$$f_{2a} = F_{2a} - f_{2b} = \left(1 - \left(h_{2a2a} + h_{2b2b} + \frac{1}{k}\right)^{-1} h_{2a2a}\right)F_{2a}$$

The direct and cross receptances for this situation (depicted in Fig. 7.2.7) are provided in Eqs. 7.2.25 through 7.2.27.

$$\begin{aligned}
H_{2a2a} &= \frac{X_{2a}}{F_{2a}} = \frac{x_{2a}}{F_{2a}} = \frac{h_{2a2a}f_{2a}}{F_{2a}} = \frac{h_{2a2a}\left(1 - \left(h_{2a2a} + h_{2b2b} + \frac{1}{k}\right)^{-1} h_{2a2a}\right)F_{2a}}{F_{2a}}\\
H_{2a2a} &= h_{2a2a} - h_{2a2a}\left(h_{2a2a} + h_{2b2b} + \frac{1}{k}\right)^{-1} h_{2a2c}
\end{aligned} \tag{7.2.25}$$

$$\begin{aligned}
H_{2b2a} &= \frac{X_{2b}}{F_{2a}} = \frac{x_{2b}}{F_{2a}} = \frac{h_{2b2b}f_{2b}}{F_{2b}} = \frac{h_{2b2b}\left(h_{2a2a} + h_{2b2b} + \frac{1}{k}\right)^{-1} h_{2a2a}F_{2a}}{F_{2a}}\\
H_{2b2a} &= h_{2b2b}\left(h_{2a2a} + h_{2b2b} + \frac{1}{k}\right)^{-1} h_{2a2a}
\end{aligned} \tag{7.2.26}$$

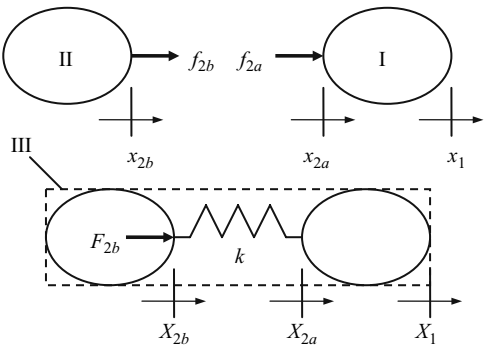

Fig. 7.2.8 Flexible coupling of components I and II to form assembly III. The force F_{2b} is applied to the assembly in order to determine H_{2b2b}, H_{2a2b}, and H_{12b}

$$H_{12a} = \frac{X_1}{F_{2a}} = \frac{x_1}{F_{2a}} = \frac{h_{12a}f_{2a}}{F_{2a}} = \frac{h_{12a}\left(1 - \left(h_{2a2a} + h_{2b2b} + \frac{1}{k}\right)^{-1} h_{2a2a}\right)F_{2a}}{F_{2a}}$$
$$H_{12a} = h_{12a} - h_{12a}\left(h_{2a2a} + h_{2b2b} + \frac{1}{k}\right)^{-1} h_{2a2a} \tag{7.2.27}$$

Our final scenario for the two component flexible coupling is shown in Fig. 7.2.8. Here, we apply the external force F_{2b} to coordinate X_{2b} to obtain the direct and cross assembly receptances H_{2b2b}, H_{2a2b}, and H_{12b}. The component displacements are the same as the previous case: $x_1 = h_{12a}f_{2a}$ and $x_{2a} = h_{2a2a}f_{2a}$ for substructure I and $x_{2b} = h_{2b2b}f_{2b}$ for substructure II. However, the equilibrium condition is modified to be $f_{2a} + f_{2b} = F_{2b}$ and the compatibility condition is rewritten as:

$$k(x_{2a} - x_{2b}) = -f_{2a}. \tag{7.2.28}$$

We find f_{2a} by substituting the component displacements in Eq. 7.2.28 and replacing f_{2b} with $F_{2a} - f_{2a}$.

$$k(h_{2a2a}f_{2a} - h_{2b2b}F_{2b} + h_{2b2h}f_{2a}) = -f_{2a}$$
$$kh_{2a2a}f_{2a} - kh_{2b2b}F_{2b} + kh_{2b2h}f_{2a} = -f_{2a}$$
$$\left(h_{2a2a} + h_{2b2b} + \frac{1}{k}\right)f_{2a} = h_{2b2b}F_{2b}$$
$$f_{2a} = \left(h_{2a2a} + h_{2b2b} + \frac{1}{k}\right)^{-1} h_{2b2b}F_{2b}$$

Again using the equilibrium condition we find the equation for f_{2b}.

$$f_{2b} = F_{2b} - f_{2a} = \left(1 - \left(h_{2a2a} + h_{2b2b} + \frac{1}{k}\right)^{-1} h_{2b2b}\right) F_{2b}$$

The direct and cross receptances for the case shown in Fig. 7.2.8 are given in Eqs. 7.2.29 through 7.2.31.

$$H_{2b2b} = \frac{X_{2b}}{F_{2b}} = \frac{x_{2b}}{F_{2b}} = \frac{h_{2b2b} f_{2b}}{F_{2b}} = \frac{h_{2b2b}\left(1 - \left(h_{2a2a} + h_{2b2b} + \frac{1}{k}\right)^{-1} h_{2b2b}\right) F_{2b}}{F_{2b}}$$
$$H_{2b2b} = h_{2b2b} - h_{2b2b}\left(h_{2a2a} + h_{2b2b} + \frac{1}{k}\right)^{-1} h_{2b2b} \tag{7.2.29}$$

$$H_{2a2b} = \frac{X_{2a}}{F_{2b}} = \frac{x_{2a}}{F_{2b}} = \frac{h_{2a2a} f_{2a}}{F_{2b}} = \frac{h_{2a2a}\left(h_{2a2a} + h_{2b2b} + \frac{1}{k}\right)^{-1} h_{2b2b} F_{2b}}{F_{2b}}$$
$$H_{2a2b} = h_{2a2a}\left(h_{2a2a} + h_{2b2b} + \frac{1}{k}\right)^{-1} h_{2b2b} \tag{7.2.30}$$

$$H_{12b} = \frac{X_1}{F_{2b}} = \frac{x_1}{F_{2b}} = \frac{h_{12a} f_{2a}}{F_{2a}} = \frac{h_{12a}\left(h_{2a2a} + h_{2b2b} + \frac{1}{k}\right)^{-1} h_{2b2b} F_{2b}}{F_{2b}}$$
$$H_{12b} = h_{12a}\left(h_{2a2a} + h_{2b2b} + \frac{1}{k}\right)^{-1} h_{2b2b} \tag{7.2.31}$$

7.2.3 Two Component Flexible, Damped Coupling[6]

As we discussed in Section 2.1, damping is always present in mechanical systems. Therefore, as a final step in our receptance coupling of bodies I and II to form assembly III, we can expand the model in Fig. 7.2.6 to include viscous damping at the coupling interface. See Fig. 7.2.9.

IN A NUTSHELL We recognize that the interface between the tool and holder, as with any common interface, is not rigid. Small relative motions between these bodies can produce damping.

[6] Author T. Schmitz gratefully acknowledges collaboration with Dr. T. Burns, National Institute of Standards and Technology, Gaithersburg, MD, in developing the damping analysis.

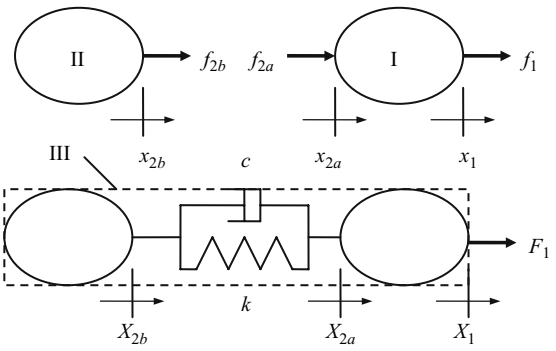

Fig. 7.2.9 Viscously damped, flexible coupling of components I and II to form assembly III. As with the two component flexible coupling case, the force F_1 is applied to the assembly in order to determine H_{11}, H_{2a1}, and H_{2b1}

The expressions for the component displacements and equilibrium conditions remain unchanged relative to the flexible coupling derivation when we add damping. However, the compatibility condition is now:

$$k(x_{2b} - x_{2a}) + i\omega c(x_{2b} - x_{2a}) = -f_{2b}, \tag{7.2.32}$$

where we have assumed harmonic motion so that the velocity dependent damping forces can be express in the form $i\omega cx$. Equation 7.2.32 can be rewritten as:

$$(k + i\omega c)(x_{2b} - x_{2a}) = -f_{2b}. \tag{7.2.33}$$

If we substitute the complex, frequency dependent variable k' for $(k + i\omega c)$, then we see that the compatibility equation takes the same form as shown in Eq. 7.2.19 and we can simply replace k in Eq. 7.2.21 with k' to obtain Eq. 7.2.34 [5]. This defines the direct FRF at coordinate X_1 on assembly III in Fig. 7.2.9. The same substitution can be made in the other assembly receptances derived for the two component flexible coupling in order to obtain the two component flexible, damped coupling results.

$$H_{11} = h_{11} - h_{12a}\left(h_{2a2a} + h_{2b2b} + \frac{1}{k'}\right)^{-1} h_{2a1} \tag{7.2.34}$$

Before proceeding with a numerical example, we present Table 7.2.1 which summarizes the receptance coupling equations developed in the previous paragraphs.

Table 7.2.1 Direct and cross receptances for two component coupling. The connection type (labeled C-type) is R, rigid, or F, flexible. The receptance type (labeled R-type) is D, direct, or C, cross. The corresponding figure and equation numbers are also included

C-type	Substructure coordinates			Receptances	Fig.	Eq.
	I	II	R-type			
R	x_{1a}	x_{1b}	D	$H_{11} = h_{1a1a} - h_{1a1a}(h_{1a1a} + h_{1b1b})^{-1} h_{1a1a}$	7.2.1	7.2.1
R	x_1, x_{2a}	x_{2b}	D	$H_{11} = h_{11} - h_{12a}(h_{2a2a} + h_{2b2b})^{-1} h_{2a1}$	7.2.2	7.2.5
			C	$H_{21} = h_{2a1} - h_{2a2a}(h_{2a2a} + h_{2b2b})^{-1} h_{2a1}$		7.2.6
			D	$H_{22} = h_{2a2a} - h_{2a2a}(h_{2a2a} + h_{2b2b})^{-1} h_{2a2a}$	7.2.3	7.2.10
			C	$H_{12} = h_{12a} - h_{12a}(h_{2a2a} + h_{2b2b})^{-1} h_{2a2a}$		7.2.11
F	x_{1a}	x_{1b}	D	$H_{1a1a} = h_{1a1a} - h_{1a1a}\left(h_{1a1a} + h_{1b1b} + \frac{1}{k}\right)^{-1} h_{1a1a}$	7.2.4	7.2.14
			C	$H_{1b1a} = h_{1b1b}\left(h_{1a1a} + h_{1b1b} + \frac{1}{k}\right)^{-1} h_{1a1a}$		7.2.15
			D	$H_{1b1b} = h_{1b1b} - h_{1b1b}\left(h_{1a1a} + h_{1b1b} + \frac{1}{k}\right)^{-1} h_{1b1b}$	7.2.5	7.2.17
			C	$H_{1a1b} = h_{1a1a}\left(h_{1a1a} + h_{1b1b} + \frac{1}{k}\right)^{-1} h_{1b1b}$		7.2.18
F	x_1, x_{2a}	x_{2b}	D	$H_{11} = h_{11} - h_{12a}\left(h_{2a2a} + h_{2b2b} + \frac{1}{k}\right)^{-1} h_{2a1}$	7.2.6	7.2.21
			C	$H_{2a1} = h_{2a1} - h_{2a2a}\left(h_{2a2a} + h_{2b2b} + \frac{1}{k}\right)^{-1} h_{2a1}$		7.2.22
			C	$H_{2b1} = h_{2b2b}\left(h_{2a2a} + h_{2b2b} + \frac{1}{k}\right)^{-1} h_{2a1}$		7.2.23
			D	$H_{2a2a} = h_{2a2a} - h_{2a2a}\left(h_{2a2a} + h_{2b2b} + \frac{1}{k}\right)^{-1} h_{2a2a}$	7.2.7	7.2.25
			C	$H_{2b2a} = h_{2b2b}\left(h_{2a2a} + h_{2b2b} + \frac{1}{k}\right)^{-1} h_{2a2a}$		7.2.26
			C	$H_{12a} = h_{12a} - h_{12a}\left(h_{2a2a} + h_{2b2b} + \frac{1}{k}\right)^{-1} h_{2a2a}$		7.2.27
			D	$H_{2b2b} = h_{2b2b} - h_{2b2b}\left(h_{2a2a} + h_{2b2b} + \frac{1}{k}\right)^{-1} h_{2b2b}$	7.2.8	7.2.29
			C	$H_{2a2b} = h_{2a2a}\left(h_{2a2a} + h_{2b2b} + \frac{1}{k}\right)^{-1} h_{2b2b}$		7.2.30
			C	$H_{12b} = h_{12a}\left(h_{2a2a} + h_{2b2b} + \frac{1}{k}\right)^{-1} h_{2b2b}$		7.2.31

IN A NUTSHELL As always, improved accuracy of the model and prediction comes at the expense of increased model complexity and/or measurement requirements. Prediction of the natural frequency of the assembly, for example, does not place the same demands on the model as prediction of the dynamic stiffness (including damping). Accurate frequency response function prediction and, by extension, the corresponding stability lobe diagram requires more care.

Example 7.2.1: Comparison of assembly modeling techniques Let's now complete an example where we compare receptance coupling to the methods we discussed in Sections 2.3 and 2.4: modal analysis and complex matrix inversion. As shown in Fig. 7.2.10, two single degree of freedom spring-mass-damper systems, I and II, are to be connected using the linear spring element, k_c, to form the new two degree of freedom assembly, III [16]. The assembled system's equations of motion are determined as shown in Sections 2.3 and 2.4. The matrix representation of these equations, after substituting the assumed harmonic form of the solution, is provided in Eq. 7.2.35. This equation takes the same form as Eq. 2.4.2, $\left(s^2[M] + s[C] + [K]\right)\{X\}e^{st} = \{F\}e^{st}$, where we've substituted the

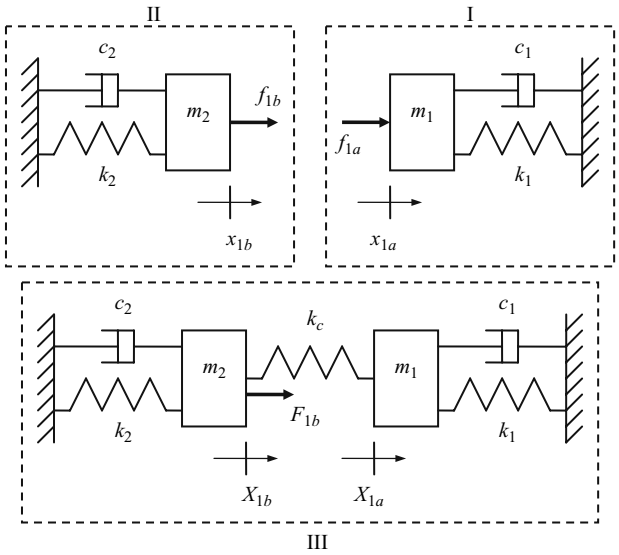

Fig. 7.2.10 Flexible coupling of spring-mass-damper systems I and II to form the two degree of freedom assembly III

Laplace variable s for the product $i\omega$ and $[M]$, $[C]$, and $[K]$ are the lumped parameter mass, damping, and stiffness matrices in local coordinates, respectively.

$$\left(s^2\begin{bmatrix} m_1 & 0 \\ 0 & m_2 \end{bmatrix} + s\begin{bmatrix} c_1 & 0 \\ 0 & c_2 \end{bmatrix} + \begin{bmatrix} k_1+k_c & -k_c \\ -k_c & k_2+k_c \end{bmatrix}\right)\begin{Bmatrix} X_{1a} \\ X_{1b} \end{Bmatrix} = \begin{Bmatrix} 0 \\ F_{1b} \end{Bmatrix}$$

$$\begin{bmatrix} m_1s^2+c_1s+(k_1+k_c) & -k_c \\ -k_c & m_2s^2+c_2s+(k_2+k_c) \end{bmatrix}\begin{Bmatrix} X_{1a} \\ X_{1b} \end{Bmatrix} = \begin{Bmatrix} 0 \\ F_{1b} \end{Bmatrix} \tag{7.2.35}$$

7.2.4 Modal Analysis

We can use the equations of motion shown in Eq. 7.2.35 to find the modal solution for the assembled system. If we assume that proportional damping exists (i.e., $[C] = \alpha[M] + \beta[K]$, where α and β are real numbers), damping can be neglected in the modal solution. Note that this solution is also independent of the external force, F_{1b}. We write the characteristic equation for this system as shown in Eq. 7.2.36. The quadratic roots of this 4th order equation, s_1^2 and s_2^2, give the two eigenvalues ($s_1^2 = -\omega_{n1}^2$ and $s_2^2 = -\omega_{n2}^2$, where $\omega_{n1} < \omega_{n2}$) for the two degree of freedom system.

$$\begin{aligned}&\left(m_1 s^2 + (k_1 + k_c)\right)\left(m_2 s^2 + (k_2 + k_c)\right) - k_c^2 = 0\\ &m_1 m_2 s^4 + (m_1(k_2 + k_c) + m_2(k_1 + k_c))s^2 + (k_1 + k_c)(k_2 + k_c) - k_c^2 = 0\end{aligned} \tag{7.2.36}$$

Substitution of these eigenvalues, normalized to the coordinate of interest (coordinate X_{1b} in this case), into either of the original equations of motion, again neglecting damping and the external force, yields the eigenvectors (mode shapes). Selecting the top equation from Eq. 7.2.35, for example, gives:

$$\frac{X_{1a}}{X_{1b}} = \frac{k_c}{m_1 s^2 + (k_1 + k_c)}. \tag{7.2.37}$$

The mass, damping, and stiffness matrices are diagonalized using the modal matrix (composed of columns of the eigenvectors), P, defined in Eq. 7.2.38. Specifically, we have that: $\left[M_q\right] = [P]^T[M][P] = \begin{bmatrix} m_{q1} & 0 \\ 0 & m_{q2} \end{bmatrix}$, $\left[C_q\right] = [P]^T[C][P] = \begin{bmatrix} c_{q1} & 0 \\ 0 & c_{q2} \end{bmatrix}$, and $\left[K_q\right] = [P]^T[K][P] = \begin{bmatrix} k_{q1} & 0 \\ 0 & k_{q2} \end{bmatrix}$. Based on these modal values, we calculate the associated damping ratios, $\zeta_{q1,2} = \frac{c_{q1,2}}{2\sqrt{k_{q1,2} m_{q1,2}}}$. The modal solution for the direct FRF at coordinate X_{1b} of the assembled system is then expressed as shown in Eq. 7.2.39, where $r_{1,2} = \frac{\omega}{\omega_{n1,2}}$.

$$P = \begin{bmatrix} \frac{X_{1a}}{X_{1b}}\left(s_1^2\right) & \frac{X_{1a}}{X_{1b}}\left(s_2^2\right) \\ 1 & 1 \end{bmatrix} \tag{7.2.38}$$

$$H_{1b1b} = \frac{X_{1b}}{F_{1b}} = \frac{1}{k_{q1}}\left(\frac{\left(1 - r_1^2\right) - i\left(2\zeta_{q1} r_1\right)}{\left(1 - r_1^2\right)^2 + \left(2\zeta_{q1} r_1\right)^2}\right) + \frac{1}{k_{q2}}\left(\frac{\left(1 - r_2^2\right) - i\left(2\zeta_{q2} r_2\right)}{\left(1 - r_2^2\right)^2 + \left(2\zeta_{q2} r_2\right)^2}\right) \tag{7.2.39}$$

7.2.5 Complex Matrix Inversion[7]

Equation 7.2.35 can be compactly written as $[A]\{X\} = \{F\}$. As shown in Section 2.4, complex matrix inversion is carried out using $\{X\}\{F\}^{-1} = [A]^{-1}$ to determine the assembly direct and cross FRFs. The inverted $[A]$ matrix for this two degree of freedom example is:

[7] As discussed in Section 2.4, complex matrix inversion, rather than modal analysis, is applied when the damping may not be proportional.

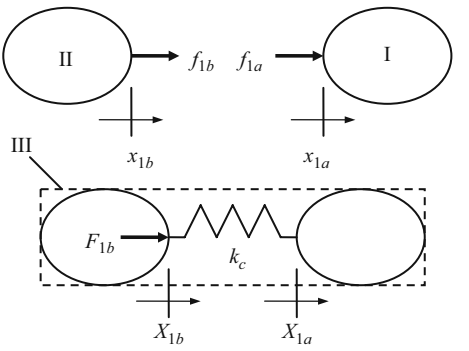

Fig. 7.2.11 Receptance coupling representation of joining spring-mass-damper systems I and II to form the two degree of freedom assembly III

$$[A]^{-1} = \frac{\begin{bmatrix} a_{22} & -a_{12} \\ -a_{21} & a_{11} \end{bmatrix}}{a_{11} \cdot a_{22} - a_{12} \cdot a_{21}} = \frac{\begin{bmatrix} -\omega^2 m_2 + i\omega c_2 + (k_2 + k_c) & k_c \\ k_c & -\omega^2 m_1 + i\omega c_1 + (k_1 + k_c) \end{bmatrix}}{(-\omega^2 m_1 + i\omega c_1 + (k_1 + k_c))(-\omega^2 m_2 + i\omega c_2 + (k_2 + k_c)) - k_c^2},$$

where we've replaced s with $i\omega$ relative to Eq. 7.2.35. The individual terms in the inverted $[A]$ matrix are:

$$[A]^{-1} = \begin{bmatrix} \frac{X_{1a}}{F_{1a}} & \frac{X_{1a}}{F_{1b}} \\ \frac{X_{1b}}{F_{1a}} & \frac{X_{1b}}{F_{1b}} \end{bmatrix} = \begin{bmatrix} H_{1a1a} & H_{1a1b} \\ H_{1b1a} & H_{1b1b} \end{bmatrix}. \tag{7.2.40}$$

7.2.6 Receptance Coupling

This case is the same as the two component flexible coupling example shown in Fig. 7.2.5. Replacing k with k_c in Eq. 7.2.17, we obtain Eq. 7.2.41. See Fig. 7.2.11.

$$\begin{aligned} \frac{X_{1b}}{F_{1b}} &= \frac{x_{1b}}{F_{1b}} = \frac{h_{1b1b} f_{1b}}{F_{1b}} = \frac{h_{1b1b}\left(1 - \left(h_{1a1a} + h_{1b1b} + \frac{1}{k_c}\right)^{-1} h_{1b1b}\right) F_{1b}}{F_{1b}} \\ \frac{X_{1b}}{F_{1b}} &= H_{1b1b} = h_{1b1b} - h_{1b1b}\left(h_{1a1a} + h_{1b1b} + \frac{1}{k_c}\right)^{-1} h_{1b1b} \end{aligned} \tag{7.2.41}$$

To compare the three methods, we select the mass, damping, and stiffness values shown in Table 7.2.2 for the model in Fig. 7.2.10. We note that proportional

Table 7.2.2 Mass, damping, and stiffness values for Ex. 7.2.1

Parameter	Value
m_1	3 kg
c_1	200 N-s/m
k_1	2×10^6 N/m
m_2	2 kg
c_2	100 N-s/m
k_2	1×10^6 N/m
k_c	5×10^5 N/m

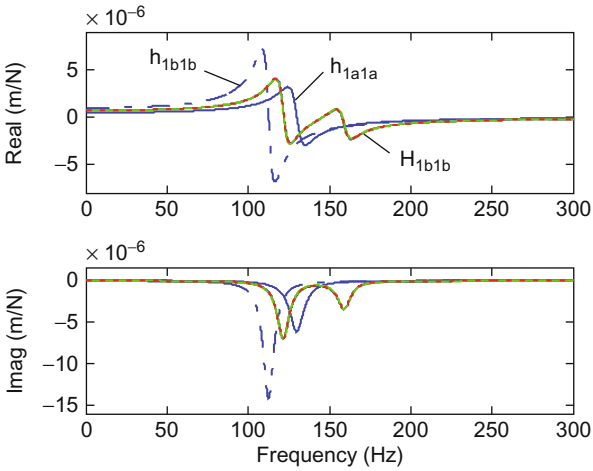

Fig. 7.2.12 Comparison of three methods for H_{1b1b} calculation. It is seen that the modal analysis, complex matrix inversion, and receptance coupling methods nominally agree (superimposed solid lines). The component receptances, h_{1a1a} and h_{1b1b}, are also shown

damping exists ($\alpha = 0$ and $\beta = 1 \times 10^{-4}$) for the selected system, so the modal approach may be applied. The MATLAB® program used to produce Fig. 7.2.12, which displays both the component receptances and the assembly receptance computed using the three methods, is provided on the companion CD as p_7_2_1_1.m. The frequency dependent differences between the complex matrix inversion result, which was obtained through vector manipulations only by calculating the H_{1b1b} result directly:

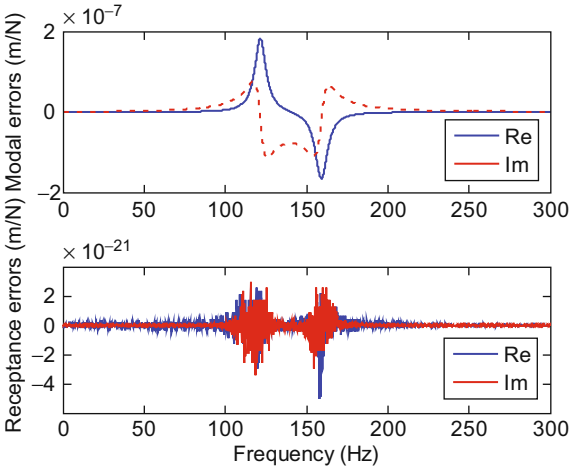

Fig. 7.2.13 Real and imaginary parts of difference between complex matrix inversion and modal analysis (top) and real and imaginary parts of difference between complex matrix inversion and receptance coupling (bottom). Receptance coupling agrees much more closely

$$H_{1b1b} = \frac{-\omega^2 m_1 + i\omega c_1 + (k_1 + k_c)}{(-\omega^2 m_1 + i\omega c_1 + (k_1 + k_c))(-\omega^2 m_2 + i\omega c_2 + (k_2 + k_c)) - k_c^2},$$

and the modal and receptance coupling method results are shown in Fig. 7.2.13. It is seen that the errors introduced by the modal method (top) are approximately 4×10^{13} times greater than the errors associated with the receptance technique (bottom). The differences between the three techniques are introduced by numerical round off errors in the mathematical manipulations. However, the improved numerical accuracy obtained with receptance coupling (vector manipulations) over modal coupling (matrix manipulations) is another benefit of the receptance coupling approach.

7.3 Advanced Receptance Coupling

The primary difference between the simple examples we've considered so far and tool-holder-spindle-machine modeling is that we now need to consider not only lateral displacements (x_i/X_i) and forces (f_j/F_j), but also rotations about lines perpendicular to the beam axis (θ_i/Θ_i) and bending couples (m_j/M_j). [8,9] To begin this discussion, let's consider the solid cylinder-prismatic cantilever beam assembly shown in Fig. 7.3.1. To determine the assembly dynamics, all four bending receptances must be included in the component descriptions (i.e., displacement-to-force, h_{ij}, displacement-to-couple, l_{ij}, rotation-to-force, n_{ij}, and rotation-to-couple, p_{ij}).

Let's summarize the steps required to predict the Fig. 7.3.1 assembly receptances.

1. Define the components and coordinates for the model. In this simple example, we can select two components: a prismatic beam with fixed-free (or cantilever) boundary conditions and a cylinder with free-free (or unsupported) boundary conditions; see Fig. 7.3.2.

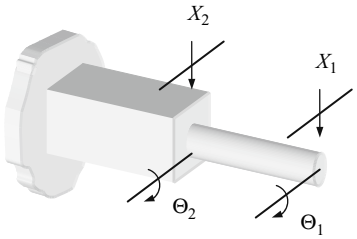

Fig. 7.3.1 Rigid coupling of solid cylinder and prismatic beam to form cantilevered assembly

[8] We will not consider axial or torsional vibrations in this analysis.

[9] Author T. Schmitz acknowledges significant collaboration with Dr. M. Davies, University of North Carolina at Charlotte, in the early application of receptance coupling to tool point FRF prediction.

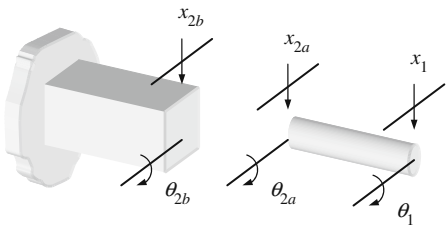

Fig. 7.3.2 Solid cylinder and prismatic beam components used to form cantilevered assembly

2. Determine the component receptances. We can use either measurements or models. For the models, an elegant choice is the closed form receptances presented by Bishop and Johnson [1] for flexural vibrations of uniform Euler-Bernoulli beams with free, fixed, sliding, and pinned boundary conditions. Of course, the Timoshenko beam model or other approaches may also be applied. See Section 7.4. For measurements, we can follow the procedures outlined in Section 2.6.
3. Based on the selected model from step 1, express the assembly receptances as a function of the component receptances. As demonstrated in Section 7.2, we determine the assembly receptances using the component displacements/rotations, equilibrium conditions, and compatibility conditions.

We begin the analysis of the system shown in Figs. 7.3.1 and 7.3.2 by writing the component receptances. Note that we have placed coordinates at the prediction location (1), which would represent the tool point for a tool-holder-spindle assembly, and coupling locations (2*a* and 2*b*). For the cylinder, we have the following direct receptances at the coordinate 1 end:

$$h_{11} = \frac{x_1}{f_1} \quad l_{11} = \frac{x_1}{m_1} \quad n_{11} = \frac{\theta_1}{f_1} \quad p_{11} = \frac{\theta_1}{m_1}. \tag{7.3.1}$$

The corresponding cross receptances at the same location are:

$$h_{12a} = \frac{x_1}{f_{2a}} \quad l_{12a} = \frac{x_1}{m_{2a}} \quad n_{12a} = \frac{\theta_1}{f_{2a}} \quad p_{12a} = \frac{\theta_1}{m_{2a}}. \tag{7.3.2}$$

At coordinate 2*a* on the cylinder, the direct and cross receptances are written as shown in Eqs. 7.3.3 and 7.3.4, respectively.

$$h_{2a2a} = \frac{x_{2a}}{f_{2a}} \quad l_{2a2a} = \frac{x_{2a}}{m_{2a}} \quad n_{2a2a} = \frac{\theta_{2a}}{f_{2a}} \quad p_{2a2a} = \frac{\theta_{2a}}{m_{2a}} \tag{7.3.3}$$

$$h_{2a1} = \frac{x_{2a}}{f_1} \quad l_{2a1} = \frac{x_{2a}}{m_1} \quad n_{2a1} = \frac{\theta_{2a}}{f_1} \quad p_{2a1} = \frac{\theta_{2a}}{m_1} \tag{7.3.4}$$

Similarly, for the prismatic beam, the direct receptances at the coupling location 2*b* are described by Eq. 7.3.5.

$$h_{2b2b} = \frac{x_{2b}}{f_{2b}} \quad l_{2b2b} = \frac{x_{2b}}{m_{2b}} \quad n_{2b2b} = \frac{\theta_{2b}}{f_{2b}} \quad p_{2b2b} = \frac{\theta_{2b}}{m_{2b}} \tag{7.3.5}$$

To simplify notation, the component receptances can be compactly represented in matrix form as shown in Eqs. 7.3.6 through 7.3.9 for the cylinder and Eq. 7.3.10 for the prismatic beam:

$$\begin{Bmatrix} x_1 \\ \theta_1 \end{Bmatrix} = \begin{bmatrix} h_{11} & l_{11} \\ n_{11} & p_{11} \end{bmatrix} \begin{Bmatrix} f_1 \\ m_1 \end{Bmatrix} \text{ or } \{u_1\} = [R_{11}]\{q_1\}, \tag{7.3.6}$$

$$\begin{Bmatrix} x_{2a} \\ \theta_{2a} \end{Bmatrix} = \begin{bmatrix} h_{2a2a} & l_{2a2a} \\ n_{2a2a} & p_{2a2a} \end{bmatrix} \begin{Bmatrix} f_{2a} \\ m_{2a} \end{Bmatrix} \text{ or } \{u_{2a}\} = [R_{2a2a}]\{q_{2a}\}, \tag{7.3.7}$$

$$\begin{Bmatrix} x_1 \\ \theta_1 \end{Bmatrix} = \begin{bmatrix} h_{12a} & l_{12a} \\ n_{12a} & p_{12a} \end{bmatrix} \begin{Bmatrix} f_{2a} \\ m_{2a} \end{Bmatrix} \text{ or } \{u_1\} = [R_{12a}]\{q_{2a}\}, \tag{7.3.8}$$

$$\begin{Bmatrix} x_{2a} \\ \theta_{2a} \end{Bmatrix} = \begin{bmatrix} h_{2a1} & l_{2a1} \\ n_{2a1} & p_{2a1} \end{bmatrix} \begin{Bmatrix} f_1 \\ m_1 \end{Bmatrix} \text{ or } \{u_{2a}\} = [R_{2a1}]\{q_1\}, \text{ and} \tag{7.3.9}$$

$$\begin{Bmatrix} x_{2b} \\ \theta_{2b} \end{Bmatrix} = \begin{bmatrix} h_{2b2b} & l_{2b2b} \\ n_{2b2b} & p_{2b2b} \end{bmatrix} \begin{Bmatrix} f_{2b} \\ m_{2b} \end{Bmatrix} \text{ or } \{u_{2b}\} = [R_{2b2b}]\{q_{2b}\}, \tag{7.3.10}$$

where R_{ij} is the generalized receptance matrix that describes both translational and rotational component behavior [6, 10, 17] and u_i and q_j are the corresponding generalized displacement/rotation and force/couple vectors. To visualize R_{ij}, we can think of each frequency dependent 2×2 R_{ij} matrix as a page in a book with every page representing a different frequency value. Flipping through the book from front to back scans the frequency values from low to high through the modeled or measured bandwidth. Naturally, all receptances in the coupling analysis must be based on the same frequency vector (resolution and range).

We write the component receptances, using the new notation, as: $u_1 = R_{11}q_1 + R_{12a}q_{2a}$ and $u_{2a} = R_{2a1}q_1 + R_{2a2a}q_{2a}$ for the cylinder, and $u_{2b} = R_{2b2b}q_{2b}$ for the prismatic beam. If we apply a rigid connection between the two components, the compatibility condition is: $u_{2b} - u_{2a} = 0$. Additionally, if we again specify that the component and assembly coordinates are at the same physical locations, then we have that $u_1 = U_1$ and $u_{2a} = u_{2b} = U_2$ (due to the rigid coupling).

We can write the assembly receptances as shown in Eq. 7.3.11, which again implements the generalized notation:

$$\begin{Bmatrix} U_1 \\ U_2 \end{Bmatrix} = \begin{bmatrix} G_{11} & G_{12} \\ G_{21} & G_{22} \end{bmatrix} \begin{Bmatrix} Q_1 \\ Q_2 \end{Bmatrix}, \tag{7.3.11}$$

where $U_i = \begin{Bmatrix} X_i \\ \Theta_i \end{Bmatrix}$, $G_{ij} = \begin{bmatrix} H_{ij} & L_{ij} \\ N_{ij} & P_{ij} \end{bmatrix}$, and $Q_j = \begin{Bmatrix} F_j \\ M_j \end{Bmatrix}$. To determine the assembly receptance at the free end of the cylinder, G_{11}, we apply Q_1 to coordinate U_1 as shown in Fig. 7.3.3, where the generalized U_i and u_i vectors

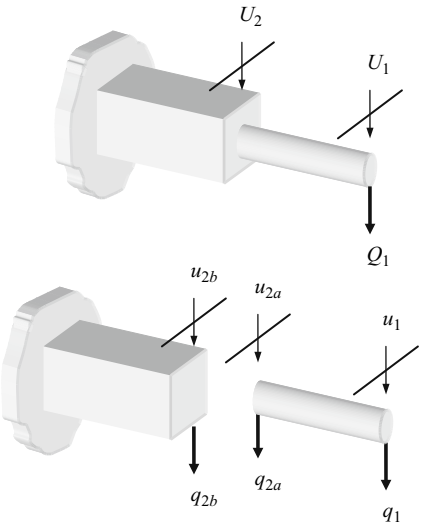

Fig. 7.3.3 Receptance coupling model for determining G_{11} and G_{21}. Rigid coupling is assumed

are shown schematically as "displacements", although we recognize that they describe both lateral translation and rotation. The associated equilibrium conditions are: $q_{2a} + q_{2b} = 0$ and $q_1 = Q_1$. By substituting the component displacements/rotations and equilibrium conditions into the compatibility condition, we obtain the expression for q_{2b} shown in Eq. 7.3.12. The component force q_{2a} is then determined from the equilibrium condition $q_{2a} = -q_{2b}$. The expression for G_{11} is given by Eq. 7.3.13. We find the corresponding cross receptance matrix, G_{21}, in a similar manner; see Eq. 7.3.14. Note that G_{11} and G_{21} comprise the first column of the receptance matrix in Eq. 7.3.11.

$$\begin{aligned} &u_{2b} - u_{2a} = 0 \\ &R_{2b2b}q_{2b} - R_{2a1}q_1 - R_{2a2a}q_{2a} = 0 \\ &(R_{2a2a} + R_{2b2b})q_{2b} - R_{2a1}Q_1 = 0 \\ &q_{2b} = (R_{2a2a} + R_{2b2b})^{-1}R_{2a1}Q_1 \end{aligned} \tag{7.3.12}$$

$$\begin{aligned} G_{11} &= \frac{U_1}{Q_1} = \frac{u_1}{Q_1} = \frac{R_{11}q_1 + R_{12a}q_{2a}}{Q_1} = \frac{R_{11}Q_1 - R_{12a}(R_{2a2a} + R_{2b2b})^{-1}R_{2a1}Q_1}{Q_1} \\ G_{11} &= R_{11} - R_{12a}(R_{2a2a} + R_{2b2b})^{-1}R_{2a1} = \begin{bmatrix} H_{11} & L_{11} \\ N_{11} & P_{11} \end{bmatrix} \end{aligned} \tag{7.3.13}$$

$$\begin{aligned} G_{21} &= \frac{U_2}{Q_1} = \frac{u_{2a}}{Q_1} = \frac{R_{2a1}q_1 + R_{2a2a}q_{2a}}{Q_1} = \frac{R_{2a1}Q_1 - R_{2a2a}(R_{2a2a} + R_{2b2b})^{-1}R_{2a1}Q_1}{Q_1} \\ G_{21} &= R_{2a1} - R_{2a2a}(R_{2a2a} + R_{2b2b})^{-1}R_{2a1} = \begin{bmatrix} H_{21} & L_{21} \\ N_{21} & P_{21} \end{bmatrix} \end{aligned} \tag{7.3.14}$$

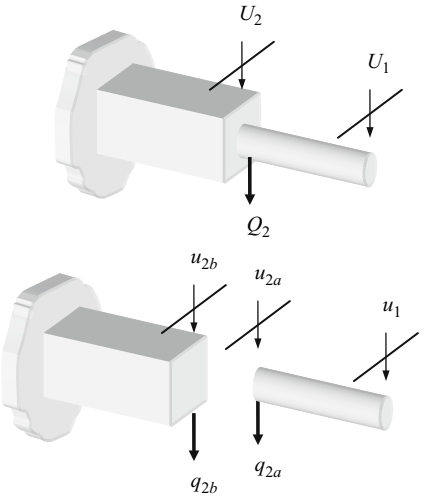

Fig. 7.3.4 Receptance coupling model for determining G_{22} and G_{12}. Rigid coupling is assumed

To find the receptances in the second column of Eq. 7.3.11, we apply Q_2 at U_2, as shown in Fig. 7.3.4. The component receptances are: $u_1 = R_{12a}q_{2a}$ and $u_{2a} = R_{2a2a}q_{2a}$ for the cylinder, and $u_{2b} = R_{2b2b}q_{2b}$ for the prismatic beam. For the assumed rigid connection the compatibility condition is again: $u_{2b} - u_{2a} = 0$. The equilibrium condition is: $q_{2a} + q_{2b} = Q_2$. By substituting the component displacements/rotations and equilibrium condition into the compatibility condition, we obtain the expression for q_{2b} shown in Eq. 7.3.15. The component force q_{2a} is then determined from the equilibrium condition $q_{2a} = Q_2 - q_{2b}$. The expression for G_{22} is provided by Eq. 7.3.16. We find the corresponding cross receptance matrix, G_{12}, in a similar manner as shown in Eq. 7.3.17.

$$\begin{aligned} &u_{2b} - u_{2a} = 0 \\ &R_{2b2b}q_{2b} - R_{2a2a}q_{2a} = 0 \\ &R_{2b2b}q_{2b} - R_{2a2a}Q_2 + R_{2a2a}q_{2b} = 0 \\ &(R_{2a2a} + R_{2b2b})q_{2b} - R_{2a2a}Q_2 = 0 \\ &q_{2b} = (R_{2a2a} + R_{2b2b})^{-1}R_{2a2a}Q_2 \end{aligned} \tag{7.3.15}$$

$$\begin{aligned} G_{22} &= \frac{U_2}{Q_2} = \frac{u_{2a}}{Q_2} = \frac{R_{2a2a}q_{2a}}{Q_2} = \frac{R_{2a2a}\left(1-(R_{2a2a}+R_{2b2b})^{-1}R_{2a2a}\right)Q_2}{Q_2} \\ G_{22} &= R_{2a2a} - R_{2a2a}(R_{2a2a} + R_{2b2b})^{-1}R_{2a2a} = \begin{bmatrix} H_{22} & L_{22} \\ N_{22} & P_{22} \end{bmatrix} \end{aligned} \tag{7.3.16}$$

Table 7.3.1 Direct and cross receptances for generalized two component coupling. The connection type (labeled C-type) is R, rigid. The receptance type (labeled R-type) is D, direct, or C, cross. The figure and equation numbers are also included. Similarities to the corresponding entries in Table 7.2.1 are evident

C-type	Substructure coordinates		Receptances		Fig.	Eq.
	I	II	R-type			
R	u_1, u_{2a}	u_{2b}	D	$G_{11} = R_{11} - R_{12a}(R_{2a2a} + R_{2b2b})^{-1} R_{2a1}$	7.3.3	7.3.13
			C	$G_{21} = R_{2a1} - R_{2a2a}(R_{2a2a} + R_{2b2b})^{-1} R_{2a1}$		7.3.14
			D	$G_{22} = R_{2a2a} - R_{2a2a}(R_{2a2a} + R_{2b2b})^{-1} R_{2a2a}$	7.3.4	7.3.16
			C	$G_{12} = R_{12a} - R_{12a}(R_{2a2a} + R_{2b2b})^{-1} R_{2a2a}$		7.3.17

$$G_{12} = \frac{U_1}{Q_2} = \frac{u_1}{Q_2} = \frac{R_{12a} q_{2a}}{Q_2} = \frac{R_{12a}\left(1 - (R_{2a2a} + R_{2b2b})^{-1} R_{2a2a}\right) Q_2}{Q_2}$$
$$G_{12} = R_{12a} - R_{12a}(R_{2a2a} + R_{2b2b})^{-1} R_{2a2a} = \begin{bmatrix} H_{12} & L_{12} \\ N_{12} & P_{12} \end{bmatrix} \tag{7.3.17}$$

We see that the procedure to model the systems with both displacement and rotations is analogous to the examples provided in Section 7.2. Let's again summarize the receptance terms in tabular form; see Table 7.3.1. Due to the clear similarities to Table 7.2.1, we will not derive the receptances for the other two component coupling cases. The only consideration is that for non-rigid coupling, we replace the scalar stiffness term, $\frac{1}{k}$, from the displacement-to-force analyses with the matrix expression $\left[\tilde{k}\right]^{-1}$, where:

$$\left[\tilde{k}\right] = \begin{bmatrix} k_{xf} & k_{\theta f} \\ k_{xm} & k_{\theta m} \end{bmatrix}.$$

The subscripts for the stiffness matrix entries indicate their function. For example, $k_{\theta f}$ represents resistance to rotation due to an applied force. As shown in Eq. 7.2.34, these four real valued stiffness terms are augmented by the corresponding damping expressions if viscous damping is included at the coupling location [11]. The new complex, frequency dependent stiffness matrix is:

$$\left[\tilde{k}'\right] = \begin{bmatrix} k_{xf} + i\omega c_{xf} & k_{\theta f} + i\omega c_{\theta f} \\ k_{xm} + i\omega c_{xm} & k_{\theta m} + i\omega c_{\theta m} \end{bmatrix}.$$

7.4 Beam Receptances

To describe the lateral vibration and associated rotation at the ends of uniform beams, we may apply Euler-Bernoulli beam theory. Many sources are available for full equation development, such as [1, 18], and we refer the reader to these texts for a detailed analysis. However, we'll review some of the basic

concepts before presenting the closed form equations developed by Bishop and Johnson [1].

For a uniform elastic beam subject to lateral vibrations, y, we can write the differential equation:

$$\frac{\partial^2 y}{\partial t^2} + \frac{EI}{\rho A}\frac{\partial^4 y}{\partial x^4} = 0 \tag{7.4.1}$$

to describe its lateral motion as a function of time, t, and position along the beam, x, where E is the beam's elastic modulus (N/m^2), I is the 2nd moment of area/area moment of inertia (m^4), ρ is the density (kg/m^3), and A is the cross sectional area (m^2). This equation assumes that the axis of the undeflected beam lies along the x direction and an infinitesimal slice of the deflected beam is bounded by plane faces. If we assume a harmonic disturbance, we can use the trial function $y = Y(x)\sin(\omega t)$, where ω is the frequency, to eliminate the time dependence. See Eq. 7.4.2, where $\lambda^4 = \omega^2 \frac{\rho A}{EI}$.

$$\frac{\partial^4 Y}{\partial x^4} - \lambda^4 Y = 0 \tag{7.4.2}$$

The general solution to Eq. 7.4.2 is given in Eq. 7.4.3. In this equation, A, B, C, and D are constants that are determined from the boundary conditions. See Table 7.4.1.

$$Y = A\cos(\lambda x) + B\sin(\lambda x) + C\cosh(\lambda x) + D\sinh(\lambda x) \tag{7.4.3}$$

Example 7.4.1: Tip receptances for clamped-free beam In this example, we'll use Eq. 7.4.3 and Table 7.4.1 to determine the receptances at the free end of a clamped-free beam. Let's first consider a harmonic force applied in the positive y direction at the free end of the uniform beam of length L as shown in Fig. 7.4.1 and find $H_{11} = \frac{Y_1}{F_1}$ and $N_{11} = \frac{\Theta_1}{F_1}$. From Table 7.4.1, the boundary conditions at coordinate 2 (clamped), where $x = 0$, are $y = 0$ and $\frac{\partial y}{\partial x} = 0$. At coordinate 1

Table 7.4.1 Boundary conditions for Euler-Bernoulli beam receptance calculations [1]

End description	Boundary conditions
Clamped	$y = 0, \frac{\partial y}{\partial x} = 0$
Free	$\frac{\partial^2 y}{\partial x^2} = 0, \frac{\partial^3 y}{\partial x^3} = 0$
Pinned	$y = 0, \frac{\partial^2 y}{\partial x^2} = 0$
Sliding	$\frac{\partial y}{\partial x} = 0, \frac{\partial^3 y}{\partial x^3} = 0$
Harmonic force $F\sin(\omega t)$	$\frac{\partial^2 y}{\partial x^2} = 0, \frac{\partial^3 y}{\partial x^3} = -\frac{F}{EI}\sin(\omega t)$
Harmonic bending couple $M\sin(\omega t)$	$\frac{\partial^2 y}{\partial x^2} = \frac{M}{EI}\sin(\omega t), \frac{\partial^3 y}{\partial x^3} = 0$

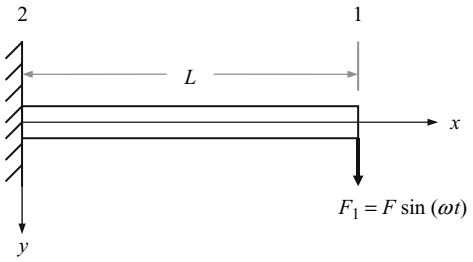

Fig. 7.4.1 Clamped-free uniform beam with a harmonic force applied at the free end

(free), where $x = L$, the boundary conditions are $\frac{\partial^2 y}{\partial x^2} = 0$ and $\frac{\partial^3 y}{\partial x^3} = -\frac{F}{EI}\sin(\omega t)$. Using these four end conditions let's determine the four coefficients A, B, C, and D in Eq. 7.4.3.

At $x = 0$, we have that $y = 0$ and $\frac{\partial y}{\partial x} = 0$. Therefore, we can use Eq. 7.4.3 directly and substitute $x = 0$ to obtain Eq. 7.4.4.

$$y|_{x=0} = Y|_{x=0} = A + C = 0 \tag{7.4.4}$$

This gives $A = -C$. Using the slope boundary condition at $x = 0$, we calculate the first derivative of Eq. 7.4.3 with respect to y and evaluate it at $x = 0$ to get Eq. 7.4.5, which yields the relationship $B = -D$.

$$\left.\frac{\partial y}{\partial x}\right|_{x=0} = \left.\frac{\partial Y}{\partial x}\right|_{x=0} = \lambda(B + D) = 0 \tag{7.4.5}$$

At $x = L$, we first apply $\frac{\partial^2 y}{\partial x^2} = 0$. See Eq. 7.4.6.

$$\left.\frac{\partial^2 y}{\partial x^2}\right|_{x=L} = \left.\frac{\partial^2 Y}{\partial x^2}\right|_{x=L} = \lambda^2\left(-A\cos(\lambda L) - B\sin(\lambda L) + C\cosh(\lambda L) + D\sinh(\lambda L)\right) = 0 \tag{7.4.6}$$

Substituting for A and B in Eq. 7.4.6, we obtain:

$$C(\cos(\lambda L) + \cosh(\lambda L)) + D(\sin(\lambda L) + \sinh(\lambda L)) = 0. \tag{7.4.7}$$

We next use $\frac{\partial^3 y}{\partial x^3} = -\frac{F}{EI}\sin(\omega t)$ at $x = L$ and again substitute for A and B to find:

$$C(-\sin(\lambda L) + \sinh(\lambda L)) + D(\cos(\lambda L) + \cosh(\lambda L)) = -\frac{F}{\lambda^3 EI}\sin(\omega t). \tag{7.4.8}$$

Let's now rewrite Eqs. 7.4.7 and 7.4.8 in matrix form and solve for the coefficients C and D. See Eq. 7.4.9.

$$\begin{bmatrix} \cos(\lambda L)+\cosh(\lambda L) & \sin(\lambda L)+\sinh(\lambda L) \\ -\sin(\lambda L)+\sinh(\lambda L) & \cos(\lambda L)+\cosh(\lambda L) \end{bmatrix} \begin{Bmatrix} C \\ D \end{Bmatrix} = \begin{Bmatrix} 0 \\ -\frac{F}{\lambda^3 EI} \end{Bmatrix} \sin(\omega t) \quad (7.4.9)$$

We can use Cramer's rule [19] to determine C and D. Writing Eq. 7.4.9 in the generic form $[A]\{x\} = \{B\}$, or $\begin{bmatrix} a_{11} & a_{12} \\ a_{21} & a_{22} \end{bmatrix} \begin{Bmatrix} x_1 \\ x_2 \end{Bmatrix} = \begin{Bmatrix} b_1 \\ b_2 \end{Bmatrix}$, we find x_1 by Eq. 7.4.10 and x_2 by 7.4.11.

$$x_1 = \frac{\begin{vmatrix} b_1 & a_{12} \\ b_2 & a_{22} \end{vmatrix}}{\begin{vmatrix} a_{11} & a_{12} \\ a_{21} & a_{22} \end{vmatrix}} = \frac{b_1 a_{22} - b_2 a_{12}}{a_{11} a_{22} - a_{21} a_{12}} \quad (7.4.10)$$

$$x_2 = \frac{\begin{vmatrix} a_{11} & b_1 \\ a_{21} & b_2 \end{vmatrix}}{\begin{vmatrix} a_{11} & a_{12} \\ a_{21} & a_{22} \end{vmatrix}} = \frac{a_{11} b_2 - a_{21} b_1}{a_{11} a_{22} - a_{21} a_{12}} \quad (7.4.11)$$

Substitution in Eq. 7.4.10 gives C, while Eq. 7.4.11 is used to find D. See Eqs. 7.4.12 and 7.4.13.

$$C = \frac{\begin{vmatrix} 0 & \sin(\lambda L)+\sinh(\lambda L) \\ -\frac{F}{\lambda^3 EI}\sin(\omega t) & \cos(\lambda L)+\cosh(\lambda L) \end{vmatrix}}{\begin{vmatrix} \cos(\lambda L)+\cosh(\lambda L) & \sin(\lambda L)+\sinh(\lambda L) \\ -\sin(\lambda L)+\sinh(\lambda L) & \cos(\lambda L)+\cosh(\lambda L) \end{vmatrix}} =$$

$$C = \frac{\frac{F}{\lambda^3 EI}(\sin(\lambda L)+\sinh(\lambda L))}{(\cos(\lambda L)+\cosh(\lambda L))^2 - (-\sin(\lambda L)+\sinh(\lambda L))(\sin(\lambda L)+\sinh(\lambda L))}\sin(\omega t) \quad (7.4.12)$$

$$C = \frac{F(\sin(\lambda L)+\sinh(\lambda L))}{2\lambda^3 EI(1+\cos(\lambda L)\cosh(\lambda L))}\sin(\omega t)$$

$$D = \frac{\begin{vmatrix} \cos(\lambda L)+\cosh(\lambda L) & 0 \\ -\sin(\lambda L)+\sinh(\lambda L) & -\frac{F}{\lambda^3 EI}\sin(\omega t) \end{vmatrix}}{\begin{vmatrix} \cos(\lambda L)+\cosh(\lambda L) & \sin(\lambda L)+\sinh(\lambda L) \\ -\sin(\lambda L)+\sinh(\lambda L) & \cos(\lambda L)+\cosh(\lambda L) \end{vmatrix}} =$$

$$D = \frac{-\frac{F}{\lambda^3 EI}(\cos(\lambda L)+\cosh(\lambda L))}{(\cos(\lambda L)+\cosh(\lambda L))^2 - (-\sin(\lambda L)+\sinh(\lambda L))(\sin(\lambda L)+\sinh(\lambda L))}\sin(\omega t) \quad (7.4.13)$$

$$D = -\frac{F(\cos(\lambda L)+\cosh(\lambda L))}{2\lambda^3 EI(1+\cos(\lambda L)\cosh(\lambda L))}\sin(\omega t)$$

We determine Y_1 by substituting the equations for C and D, together with the relationships $A = -C$ and $B = -D$, in Eq. 7.4.3. Because $x = L$ at coordinate 1, we also substitute L for x. The result is provided in Eq. 7.4.14.

$$\begin{aligned}
Y_1 &= A\cos(\lambda L) + B\sin(\lambda L) + C\cosh(\lambda L) + D\sinh(\lambda L)\\
Y_1 &= -C\cos(\lambda L) - D\sin(\lambda L) + C\cosh(\lambda L) + D\sinh(\lambda L)\\
Y_1 &= C(-\cos(\lambda L) + \cosh(\lambda L)) + D(-\sin(\lambda L) + \sinh(\lambda L))\\
Y_1 &= \frac{F(\sin(\lambda L) + \sinh(\lambda L))}{2\lambda^3 EI(1 + \cos(\lambda L)\cosh(\lambda L))}\sin(\omega t)(-\cos(\lambda L) + \cosh(\lambda L)) -\\
&\quad \frac{F(\cos(\lambda L) + \cosh(\lambda L))}{2\lambda^3 EI(1 + \cos(\lambda L)\cosh(\lambda L))}\sin(\omega t)(-\sin(\lambda L) + \sinh(\lambda L))\\
Y_1 &= -\left(\begin{array}{c}\frac{(\sin(\lambda L) + \sinh(\lambda L))(\cos(\lambda L) - \cosh(\lambda L))}{2\lambda^3 EI(1 + \cos(\lambda L)\cosh(\lambda L))} -\\ \frac{(\cos(\lambda L) + \cosh(\lambda L))(\sin(\lambda L) - \sinh(\lambda L))}{2\lambda^3 EI(1 + \cos(\lambda L)\cosh(\lambda L))}\end{array}\right) F\sin(\omega t)
\end{aligned} \tag{7.4.14}$$

Finally, the displacement-to-force tip receptance at the free end of the beam is written as shown in Eq. 7.4.15.

$$\begin{aligned}
H_{11} = \frac{Y_1}{F_1} &= \frac{-\left(\begin{array}{c}\frac{(\sin(\lambda L) + \sinh(\lambda L))(\cos(\lambda L) - \cosh(\lambda L))}{2\lambda^3 EI(1 + \cos(\lambda L)\cosh(\lambda L))} -\\ \frac{(\cos(\lambda L) + \cosh(\lambda L))(\sin(\lambda L) - \sinh(\lambda L))}{2\lambda^3 EI(1 + \cos(\lambda L)\cosh(\lambda L))}\end{array}\right) F\sin(\omega t)}{F\sin(\omega t)}\\
H_{11} &= -\left(\begin{array}{c}\frac{(\sin(\lambda L) + \sinh(\lambda L))(\cos(\lambda L) - \cosh(\lambda L))}{2\lambda^3 EI(1 + \cos(\lambda L)\cosh(\lambda L))} -\\ \frac{(\cos(\lambda L) + \cosh(\lambda L))(\sin(\lambda L) - \sinh(\lambda L))}{2\lambda^3 EI(1 + \cos(\lambda L)\cosh(\lambda L))}\end{array}\right)\\
H_{11} &= \frac{\sin(\lambda L)\cosh(\lambda L) - \cos(\lambda L)\sinh(\lambda L)}{\lambda^3 EI(1 + \cos(\lambda L)\cosh(\lambda L))}
\end{aligned} \tag{7.4.15}$$

To determine the rotation-to-force tip receptance, we return to Eq. 7.4.3 and substitute for A, B, C, and D.

$$Y = (C(-\cos(\lambda x) + \cosh(\lambda x)) + D(-\sin(\lambda x) + \sinh(\lambda x))) \tag{7.4.16}$$

We then obtain rotation by differentiating Y with respect to x, $\Theta = \frac{dY}{dx}$, and evaluate this expression at $x = L$. Finally, we divide this result by F_1 to find $N_{11} = \frac{\Theta_1}{F_1}$. See Eq. 7.4.17.

$$N_{11} = \frac{\sin(\lambda L)\sinh(\lambda L)}{\lambda^2 EI(1 + \cos(\lambda L)\cosh(\lambda L))} \tag{7.4.17}$$

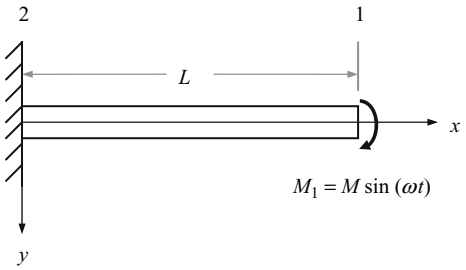

Fig. 7.4.2 Clamped-free uniform beam with a harmonic bending couple applied at the free end

The remaining tip receptances are $L_{11} = \frac{Y_1}{M_1}$ and $P_{11} = \frac{\Theta_1}{M_1}$. We find these terms by applying the harmonic bending couple $M_1 = M\sin(\omega t)$ at coordinate 1 as shown in Fig. 7.4.2. The boundary conditions at coordinate 2 ($x = 0$) are $y = 0$ and $\frac{\partial y}{\partial x} = 0$. The boundary conditions at coordinate 1 ($x = L$) are $\frac{\partial^2 y}{\partial x^2} = \frac{M}{EI}\sin(\omega t)$ and $\frac{\partial^3 y}{\partial x^3} = 0$. We find the coefficients A, B, C, and D from Eq. 7.4.3 in the same manner as described in the previous paragraphs.

At $x = 0$, the situation is identical to the force application case shown in Fig. 7.4.1 so we obtain $A = -C$ and $B = -D$. At $x = L$, we first use $\frac{\partial^2 y}{\partial x^2} = \frac{M}{\lambda^2 EI}$ as demonstrated in Eq. 7.4.18.

$$\left.\frac{\partial^2 y}{\partial x^2}\right|_{x=L} = \left.\frac{\partial^2 Y}{\partial x^2}\right|_{x=L} = \lambda^2\begin{pmatrix} -A\cos(\lambda L) - B\sin(\lambda L) + \\ C\cosh(\lambda L) + D\sinh(\lambda L) \end{pmatrix} = \frac{M}{\lambda^2 EI}\sin(\omega t) \quad (7.4.18)$$

Substitution for A and B in Eq. 7.4.18 gives:

$$C(\cos(\lambda L) + \cosh(\lambda L)) + D(\sin(\lambda L) + \sinh(\lambda L)) = \frac{M}{\lambda^2 EI}\sin(\omega t). \quad (7.4.19)$$

We next apply $\frac{\partial^3 y}{\partial x^3} = 0$ (at $x = L$) and substitute for A and B to get:

$$C(-\sin(\lambda L) + \sinh(\lambda L)) + D(\cos(\lambda L) + \cosh(\lambda L)) = 0. \quad (7.4.20)$$

Expressing Eqs. 7.4.19 and 7.4.20 in matrix form yields:

$$\begin{bmatrix} \cos(\lambda L) + \cosh(\lambda L) & \sin(\lambda L) + \sinh(\lambda L) \\ -\sin(\lambda L) + \sinh(\lambda L) & \cos(\lambda L) + \cosh(\lambda L) \end{bmatrix} \begin{Bmatrix} C \\ D \end{Bmatrix} = \begin{Bmatrix} \frac{M}{\lambda^2 EI} \\ 0 \end{Bmatrix} \sin(\omega t). \quad (7.4.21)$$

Again applying Cramer's rule, we obtain equations for C and D.

$$C = \frac{M(\cos(\lambda L) + \cosh(\lambda L))}{2\lambda^2 EI(1 + \cos(\lambda L)\cosh(\lambda L))}\sin(\omega t) \tag{7.4.22}$$

$$D = -\frac{M(-\sin(\lambda L) + \sinh(\lambda L))}{2\lambda^2 EI(1 + \cos(\lambda L)\cosh(\lambda L))}\sin(\omega t) \tag{7.4.23}$$

We find Y_1 by substituting Eqs. 7.4.22 and 7.4.23, together with the relationships $A = -C$ and $B = -D$, in Eq. 7.4.3. We also set $x = L$. The result is given in Eq. 7.4.24.

$$Y_1 = -\left(\begin{array}{c}\dfrac{(\cos(\lambda L) + \cosh(\lambda L))(\cos(\lambda L) - \cosh(\lambda L))}{2\lambda^2 EI(1 + \cos(\lambda L)\cosh(\lambda L))} + \\ \dfrac{(\sin(\lambda L) - \sinh(\lambda L))(\sin(\lambda L) - \sinh(\lambda L))}{2\lambda^2 EI(1 + \cos(\lambda L)\cosh(\lambda L))}\end{array}\right) M\sin(\omega t) \tag{7.4.24}$$

We obtain the displacement-to-couple tip receptance at the free end of the beam by dividing Eq. 7.4.24 by M_1. A comparison of Eqs. 7.4.25 and 7.4.17 shows us that the displacement-to-couple and rotation-to-force receptances are identical.

$$L_{11} = \frac{Y_1}{M_1}\frac{-\left(\begin{array}{c}\dfrac{(\cos(\lambda L) + \cosh(\lambda L))(\cos(\lambda L) - \cosh(\lambda L))}{2\lambda^2 EI(1 + \cos(\lambda L)\cosh(\lambda L))} + \\ \dfrac{(\sin(\lambda L) - \sinh(\lambda L))(\sin(\lambda L) - \sinh(\lambda L))}{2\lambda^2 EI(1 + \cos(\lambda L)\cosh(\lambda L))}\end{array}\right) M\sin(\omega t)}{M\sin(\omega t)}$$

$$L_{11} = -\left(\begin{array}{c}\dfrac{(\cos(\lambda L) + \cosh(\lambda L))(\cos(\lambda L) - \cosh(\lambda L))}{2\lambda^2 EI(1 + \cos(\lambda L)\cosh(\lambda L))} + \\ \dfrac{(\sin(\lambda L) - \sinh(\lambda L))(\sin(\lambda L) - \sinh(\lambda L))}{2\lambda^2 EI(1 + \cos(\lambda L)\cosh(\lambda L))}\end{array}\right) \tag{7.4.25}$$

$$L_{11} = \frac{\sin(\lambda L)\sinh(\lambda L)}{\lambda^2 EI(1 + \cos(\lambda L)\cosh(\lambda L))}$$

To determine the rotation-to-couple tip receptance, we return to Eq. 7.4.3 and substitute for A, B, C, and D (according to Eqs. 7.4.22 and 7.4.23).

$$Y = (C(-\cos(\lambda x) + \cosh(\lambda x)) + D(-\sin(\lambda x) + \sinh(\lambda x))) \tag{7.4.26}$$

We then find $P_{11} = \frac{\Theta_1}{M_1}$ by: 1) differentiating Y with respect to x to obtain rotation $\Theta = \frac{dY}{dx}$; 2) evaluating this expression at $x = L$; and 3) dividing this result by M_1. See Eq. 7.4.27.

$$P_{11} = \frac{\sin(\lambda L)\cosh(\lambda L) + \cos(\lambda L)\sinh(\lambda L)}{\lambda EI(1 + \cos(\lambda L)\cosh(\lambda L))} \tag{7.4.27}$$

This process can be repeated for any of the boundary conditions shown in Table 7.4.1. The tip receptance results for clamped-free and free-free conditions

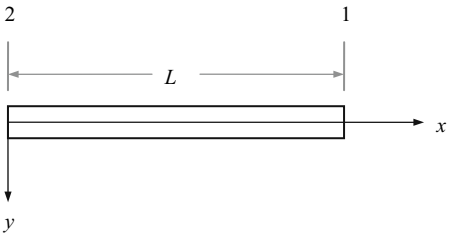

Fig. 7.4.3 Free-free uniform beam

Table 7.4.2 Euler-Bernoulli beam tip receptances for clamped-free and free-free boundary conditions [1]. Coordinates 1 and 2 are defined in Figs. 7.4.1 through 7.4.3. Also, $\lambda^4 = \omega^2 \frac{\rho A}{EI}$ and L is the beam length

H_{22}	N_{22}	H_{12}	N_{12}	P_{22}	L_{12}	P_{12}	H_{11}	N_{11}	P_{11}
	L_{22}	H_{21}	L_{21}		N_{21}	P_{21}		L_{11}	
Free-free									
$\frac{-c_1}{\lambda^3 c_7}$	$\frac{-c_2}{\lambda^2 c_7}$	$\frac{c_3}{\lambda^3 c_7}$	$\frac{c_4}{\lambda^2 c_7}$	$\frac{c_5}{\lambda c_7}$	$\frac{-c_4}{\lambda^2 c_7}$	$\frac{c_6}{\lambda c_7}$	$\frac{-c_1}{\lambda^3 c_7}$	$\frac{c_2}{\lambda^2 c_7}$	$\frac{c_5}{\lambda c_7}$
Clamped-free									
–	–	–	–	–	–	–	$\frac{-c_1}{\lambda^3 c_8}$	$\frac{c_2}{\lambda^2 c_8}$	$\frac{c_5}{\lambda c_8}$

Terms c_1 through c_8

$c_1 = \cos(\lambda L)\sinh(\lambda L) - \sin(\lambda L)\cosh(\lambda L)$ $\quad$ $c_5 = \cos(\lambda L)\sinh(\lambda L) + \sin(\lambda L)\cosh(\lambda L)$

$c_2 = \sin(\lambda L)\sinh(\lambda L)$ $\quad$ $c_6 = \sin(\lambda L) + \sinh(\lambda L)$

$c_3 = \sin(\lambda L) - \sinh(\lambda L)$ $\quad$ $c_7 = EI(\cos(\lambda L)\cosh(\lambda L) - 1)$

$c_4 = \cos(\lambda L) - \cosh(\lambda L)$ $\quad$ $c_8 = EI(\cos(\lambda L)\cosh(\lambda L) + 1)$

(see Fig. 7.4.3) are summarized in Table 7.4.2, where both direct and cross receptances are included for the free-free beam. No cross receptances are shown for the clamped-free beam because the response at the tip is zero for any excitation at the clamped end and the response is always zero at the clamped end. We should note that the free-free receptances also include the two (zero frequency) rigid body modes for the uniform beam. The first displacement-to-force rigid body mode, for example, represents the motion of the unsupported beam (imagine the beam floating in space) when a force is applied at its mass center and rigid body translation occurs. The second rigid body mode corresponds to a force applied at any other location, which causes rigid body rotation about the mass center.

An important omission for the receptance expressions provided in Table 7.4.2 is damping. Because we are considering solid beams under lateral vibration, the energy dissipation occurs within the beam only; there are no joints to introduce damping. As discussed in Section 2.1, internal damping is typically classified as solid, or structural, damping [20]. It is conveniently included in our harmonic vibration analysis by replacing EI in λ, c_7, and c_8 with the complex stiffness term $EI(1 + i\eta)$, where η is the solid damping factor. Representative values for selected engineering materials are provided in [21]. For tool-holder modeling, typical values for steel and sintered carbide components are in the 0.001 to 0.002 range.

While the closed form Euler-Bernoulli beam tip receptances provided in Table 7.4.2 are convenient to apply, accurate solutions are obtained only for

beams which exhibit small cross sectional area to length ratios (i.e., long slender beams). An alternative for beams that do not meet this criterion is the Timoshenko beam model [22]. The corresponding differential equation is given by:

$$\left(\frac{\partial^2 y}{\partial t^2}+\frac{EI}{\rho A}\frac{\partial^4 y}{\partial x^4}\right)+\left(\frac{\rho I}{\hat{k}AG}\frac{\partial^4 y}{\partial t^4}+\frac{EI}{\hat{k}AG}\frac{\partial^4 y}{\partial x^2\partial t^2}\right)-\left(\frac{I}{A}\frac{\partial^4 y}{\partial x^2\partial t^2}\right)=0, \qquad (7.4.28)$$

where $\hat{k}$ is a shape factor that depends on the beam cross section [23] and G is the shear modulus. Equation 7.4.28 is grouped into three sections (i.e., three parenthetical expressions). We see that the first section matches the Euler-Bernoulli beam equation provided in Eq. 7.4.1. The second and third sections account for shear deformations and rotary inertia, respectively. While these additional terms improve the model accuracy (particularly at higher frequencies), the tradeoff is that a closed form solution is unavailable. Finite element calculations may be applied, but at the expense of computation time. A description of the Timoshenko free-free beam receptances obtained from finite element calculations is given in [24].

7.5 Assembly Receptance Predictions

In Sections 7.3 and 7.4, we provided the building blocks for assembly receptance predictions. In this section, we'll detail coupling examples to demonstrate their implementation.

Example 7.5.1: Free-free beam coupled to rigid support As a test of the receptance coupling procedure, let's couple a free-free beam to a rigid support (i.e., a wall) to verify that it matches the clamped-free beam response we derived in Section 7.4. As described in Section 7.3, we have three primary tasks to complete in order to predict the assembly response. First, we must define the components and coordinates for the model. Here we have two components: a uniform beam with free-free boundary conditions and a rigid support (which exhibits zero receptances); see Fig. 7.5.1. Second, we need to determine the component receptances. We will apply the closed form receptances provided in Table 7.4.2. Third, based on the selected model, we express the assembly receptances as a function of the component receptances as shown in Table 7.3.1.

Let's define the free-free beam to be a solid steel cylinder with a diameter of 10 mm and a length of 125 mm. The elastic modulus is 200 GPa and the density is 7800 kg/m^3. We'll select the solid damping factor to be 0.01 for plotting purposes, but in practice a value near 0.001 would be more realistic. The free-free cylinder's direct and cross receptance equations are given in Table 7.4.2, while the wall receptances are zero. To calculate λ, we need the frequency vector ω (rad/s), cross sectional area, A, and second moment of area, I. We'll use a frequency range of 5000 Hz with a resolution of 0.1 Hz. The variables A and I are defined in Eqs. 7.5.1

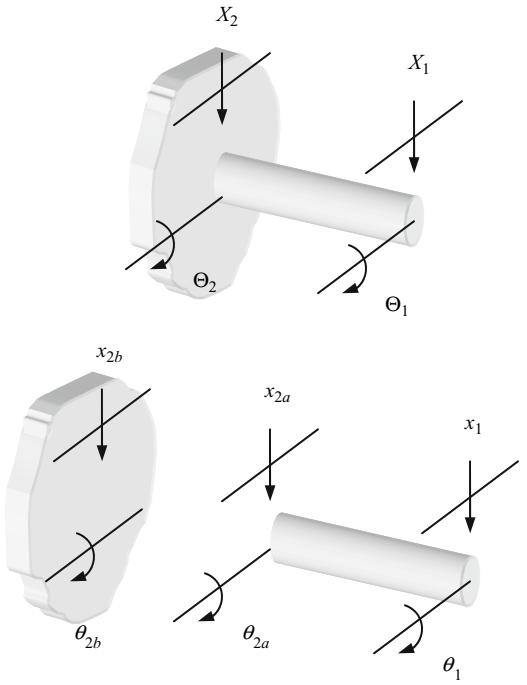

Fig. 7.5.1 Rigid coupling of the free-free cylinder to a wall

and 7.5.2 for the cylinder, where d is the cylinder diameter. The displacement-to-force free-free receptance for the cylinder, h_{11}, is shown in Fig. 7.5.2. We see a first bending natural frequency of 2884.9 Hz. The rigid body behavior is exhibited as the dramatic change in the real part as the frequency approaches zero.

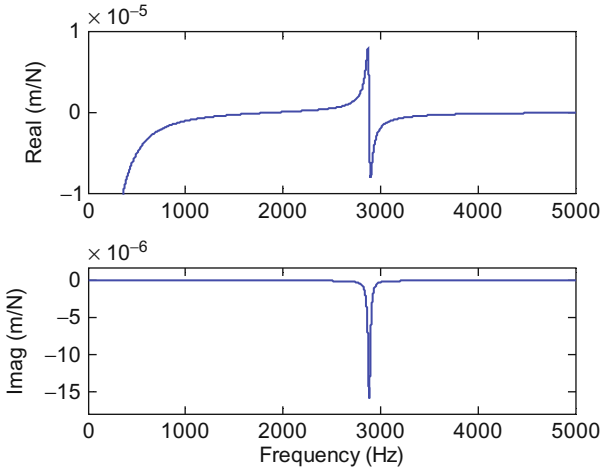

Fig. 7.5.2 Free-free receptance, h_{11}, for 10 mm diameter by 125 mm long steel cylinder

$$A = \frac{\pi d^2}{4} \tag{7.5.1}$$

$$I = \frac{\pi d^4}{64} \tag{7.5.2}$$

To rigidly couple the free-free cylinder to the wall, we apply Eq. 7.3.13:

$$G_{11} = \begin{bmatrix} H_{11} & L_{11} \\ N_{11} & P_{11} \end{bmatrix} = R_{11} - R_{12a}(R_{2a2a} + R_{2b2b})^{-1} R_{2a1},$$

where the generalized receptance matrices R_{11}, R_{12a}, R_{2a2a}, and R_{2a1} correspond to the cylinder and R_{2b2b} characterizes the wall response. The MATLAB® program p_7_5_1_1.m is used to complete the receptance coupling procedure. The results are displayed in Figs. 7.5.3 and 7.5.4. Figure 7.5.3 shows the H_{11} response from the $G_{11}(1,1)$ position (solid line). The dotted line in the figure is the clamped-free response, $H_{11} = \frac{-c_1}{\lambda^3 c_8}$, from Table 7.4.2. We see that the two curves are identical and the rigid body behavior is no longer present due to the coupling conditions. A limited frequency range is displayed in Fig. 7.5.3 to enable close comparison of the first bending mode. However, all bending modes are included in the Euler-Bernoulli beam receptances. The frequency range is increased in Fig. 7.5.4 to show the first two assembly bending modes. The vertical axis (response magnitude) is logarithmic in this plot because the second mode magnitude is much smaller than the first. Again, we observe exact agreement between the receptance coupling result (solid) and clamped-free receptance (dotted). An interesting aspect of Fig. 7.5.4 is that, in addition to the two resonant peaks at 453.4 Hz and 2841.4 Hz, we also see an "anti-resonance" at

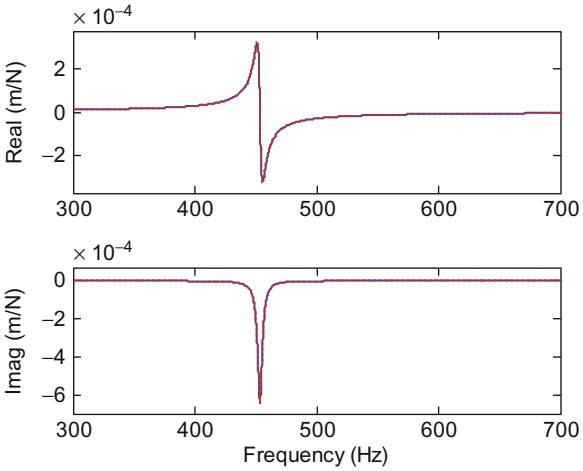

Fig. 7.5.3 Comparison of H_{11} receptance coupling result (solid line) and clamped-free response (dotted) for 10 mm diameter by 125 mm long steel cylinder

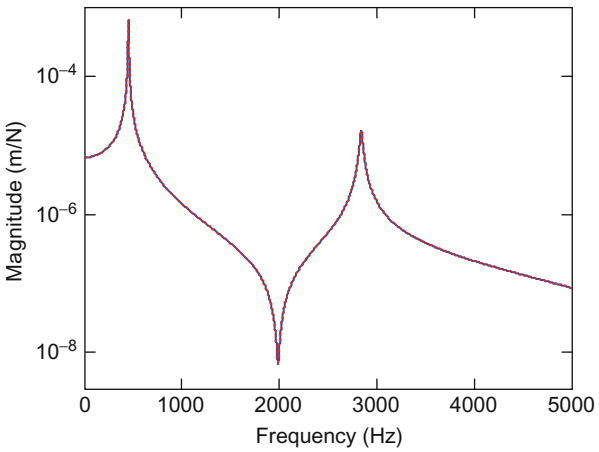

Fig. 7.5.4 Semi-logarithmic plot showing the first two bending modes for H_{11} tip receptances obtained from: 1) rigid coupling of free-free beam to wall (solid line); and 2) clamped-free response (dotted)

1988.1 Hz. At this frequency, the response is very small, even for large input force magnitudes.

The rotation-to-couple tip receptance determined from the rigid free-free beam coupling to the wall is also calculated in p_7_5_1_1.m. This $G_{11}(2,2)$ entry is shown in Fig. 7.5.5 (solid line). The clamped-free response (dotted line), $P_{11} = \frac{c_5}{\lambda c_8}$, again agrees with the receptance coupling result. We also see that the first mode natural frequency matches the H_{11} result

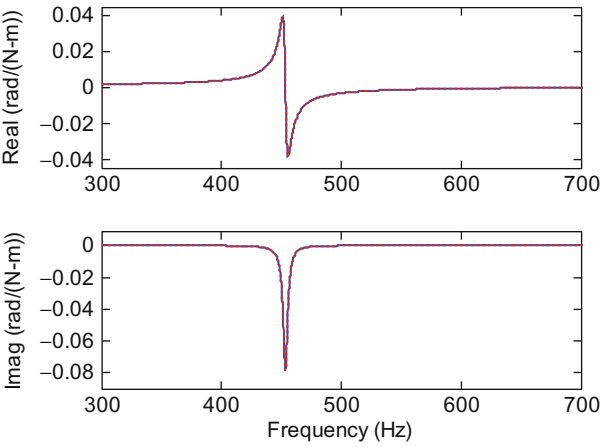

Fig. 7.5.5 Comparison of P_{11} receptance coupling result (solid line) and clamped-free response (dotted) for 10 mm diameter by 125 mm long steel cylinder

(453.4 Hz), but the magnitude is quite different; note the new units of rad/(N-m).

We've already noted that the assembly cross receptances, G_{12} and G_{21}, and the direct receptances at the clamped end, G_{22}, are zero. We can verify this by direct application of Eqs. 7.3.14, 7.3.16, and 7.3.17. For the clamped end direct receptance, Eq. 7.3.16 simplifies as shown in Eq. 7.5.3.

$$\begin{aligned} G_{22} &= R_{2a2a} - R_{2a2a}(R_{2a2a} + R_{2b2b})^{-1} R_{2a2a} \\ G_{22} &= R_{2a2a} - R_{2a2a}\left(R_{2a2a} + \begin{bmatrix} 0 & 0 \\ 0 & 0 \end{bmatrix}\right)^{-1} R_{2a2a} \\ G_{22} &= R_{2a2a} - R_{2a2a}(R_{2a2a})^{-1} R_{2a2a} = R_{2a2a} - R_{2a2a} = 0 \end{aligned} \tag{7.5.3}$$

Similar results are obtained for the cross receptances in Eqs. 7.3.14 and 7.3.17 when substituting $R_{2b2b} = \begin{bmatrix} 0 & 0 \\ 0 & 0 \end{bmatrix}$.

Example 7.5.2: Free-free beam coupled to clamped-free beam Let's now consider the case depicted in Fig. 7.3.3. A 10 mm diameter by 100 mm long steel cylinder (free-free boundary conditions) is to be rigidly coupled to a clamped-free 50 mm by 50 mm by 200 mm long steel prismatic beam. The steel elastic modulus, density, and solid damping factor are 200 GPa, 7800 kg/m^3, and 0.01, respectively. (Again, we selected the solid damping value to be artificially high for display purposes.) The analysis is the same as Ex. 7.5.1 except that the R_{2b2b} receptances are no longer zero. They are now defined as shown in Table 7.4.2, $H_{11} = \frac{-c_1}{\lambda^3 c_8}$, $L_{11} = N_{11} = \frac{c_2}{\lambda^2 c_8}$, and $P_{11} = \frac{c_5}{\lambda c_8}$. We'll again use a frequency range of 5000 Hz with a resolution of 0.1 Hz to calculate λ. The variables A and I are defined in Eqs. 7.5.4 and 7.5.5 for the square prismatic beam, where s is the side length of 50 mm. The displacement-to-force free-free receptance for the cylinder, h_{11}, is shown in Fig. 7.5.6 (solid line). The clamped-free square beam tip receptance, h_{2b2b}, is also displayed (dotted line). We see a first bending natural frequency of 4507.6 Hz for the free-free beam. The clamped-free beam has a first bending frequency of 1022.5 Hz.

$$A = s^2 \tag{7.5.4}$$

$$I = \frac{s^4}{12} \tag{7.5.5}$$

The application of Eq. 7.3.13 to this scenario using program p_7_5_2_1.m gives Fig. 7.5.7, which shows H_{11} for the assembly. We see two modes within the 5000 Hz frequency range: one at 1045.2 Hz, near the original clamped-free response, and a second more flexible mode at 680.9 Hz due to the now coupled cylinder. Because the prismatic beam is much stiffer than the cylinder, it appears to serve as a nearly rigid support for the cylinder. This may lead us to believe that approximating the assembly as a cylinder clamped to a wall is adequate. However, let's investigate

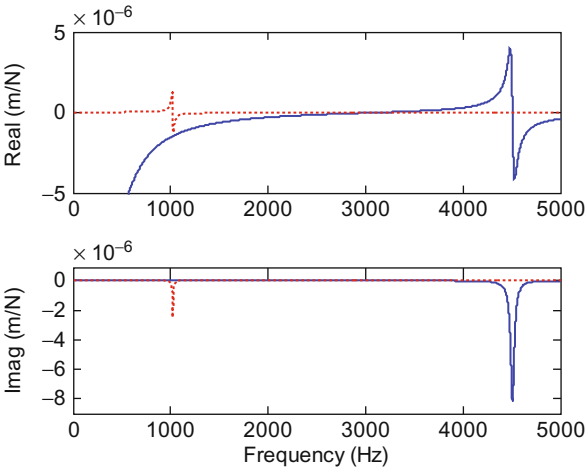

Fig. 7.5.6 Free-free receptance, h_{11}, for 10 mm diameter by 100 mm long steel cylinder (solid line) and clamped-free receptance, h_{2b2b}, for 50 mm square by 200 mm long steel prismatic beam (dotted line)

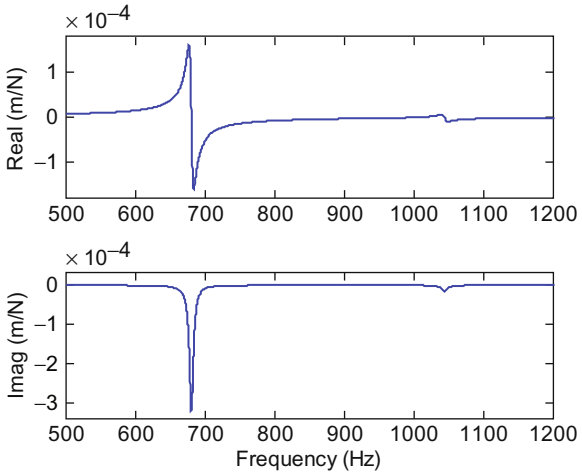

Fig. 7.5.7 Assembly displacement-to-force tip receptance H_{11} for the rigidly coupled cylinder and prismatic beam shown in Fig. 7.3.3

what happens if we modify the prismatic beam to reduce its first bending frequency to a value near the clamped-free cylinder's first bending frequency.

Figure 7.5.8 displays h_{11} for the free-free cylinder (solid line), as well as h_{2b2b} for a longer clamped-free prismatic beam (dotted line). The cylinder's first bending natural frequency remains at 4507.6 Hz for the free-free boundary conditions. However, the first bending frequency for the extended clamped-free beam is reduced to 654.4 Hz. Figure 7.5.9 shows H_{11} for the cylinder rigidly coupled to a 50 mm square by 250 mm long prismatic beam. The response is now quite different than the assembly receptance shown in Fig. 7.5.7 for the 200 mm long prismatic beam. Even though the cylinder is coupled to a more flexible base (i.e., a longer clamped-free

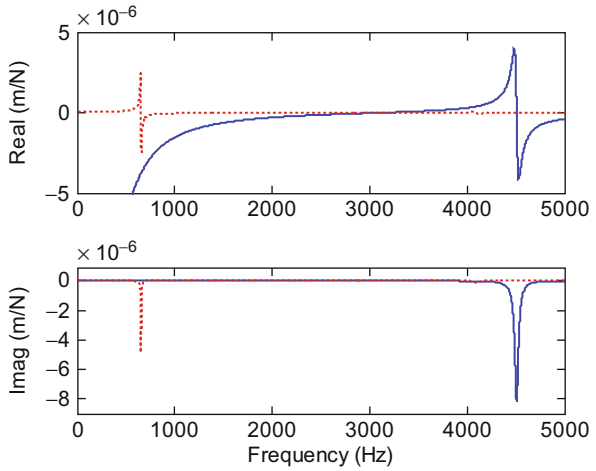

Fig. 7.5.8 Free-free receptance, h_{11}, for 10 mm diameter by 100 mm long steel cylinder (solid line) and clamped-free receptance, h_{2b2b}, for 50 mm square by 250 mm long steel prismatic beam (dotted line)

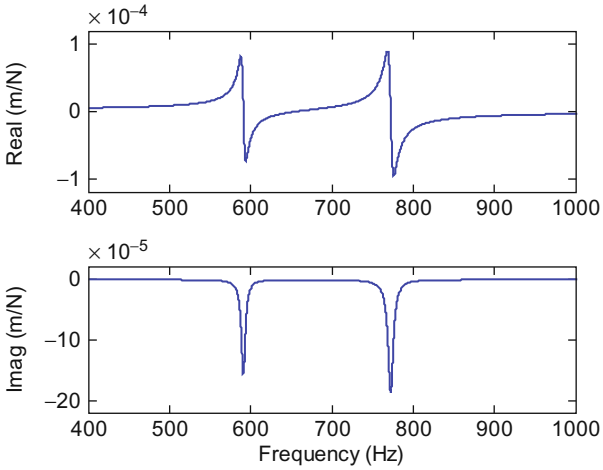

Fig. 7.5.9 The displacement-to-force tip receptance, H_{11}, for rigid coupling of the 10 mm diameter by 100 mm long cylinder to the 50 mm square by 250 mm long prismatic beam is displayed

beam), the assembly response has a smaller peak magnitude. The minimum imaginary value for the new assembly is -1.865×10^{-4} m/N, while the corresponding value for the shorter (and stiffer) prismatic beam assembly is -3.222×10^{-4} m/N; this represents a 42% compliance[10] reduction. The compliance reduction, or

[10] Compliance is the inverse of stiffness.

equivalently the stiffness increase, is due to interaction between the two beams in a manner analogous to the well known dynamic absorber. When the clamped-free prismatic beam's natural frequency is near the coupled cylinder's natural frequency, some energy is able to "pass through" the cylinder and excite the stiffer base. The result is that the energy is more equally partitioned between the two modes and the assembly response appears stiffer [8]. An electrical equivalent is the impedance matching strategy used at cable connections. For example, it is common to use 50 Ω terminations at all connections to encourage signal transmission and avoid reflection.

One application of this phenomenon is to select tool lengths that encourage the interaction between the clamped-free tool's first bending frequency and one of the spindle natural frequencies (in bending). For slender tools, as the tool overhang length from the holder face is adjusted, its natural frequency can be modified to match a spindle natural frequency. This technique, referred to as "tool length tuning" or simply "tool tuning" [8, 25, 26], can lead to improved dynamic stiffness (i.e., a smaller magnitude for the tool point FRF) and increased allowable axial depths of cut. As we saw with the prismatic beam-cylinder coupling, the surprising outcome is that increasing the tool length can reduce the assembly compliance in some instances. We should also note that forcing this interaction and encouraging the two mode response shown in Fig. 7.5.9 will generally lead to competing lobes (Section 3.4) in the corresponding stability lobe diagram.

7.6 Tool-Holder-Spindle-Machine Receptance Predictions[11]

As we noted in Section 7.2, we can consider the tool-holder-spindle-machine combination as being composed of three parts: the tool, holder, and spindle-machine [7]. This enables us to use the closed form Euler-Bernoulli beam receptances contained in Table 7.4.2 to describe the tool and holder dynamics; finite element based Timoshenko beam receptances may also be applied, of course. Due to modeling challenges, we measure the spindle-machine response using impact testing techniques. Given the component responses, we then couple their individual FRFs to obtain the assembly response via the receptance coupling substructure analysis (RCSA) approach [7]. Let's now discuss this procedure in more detail.

Figure 7.6.1 depicts our model composed of the three individual components: I – tool, II – holder, and III – spindle-machine[12]. So far we have not discussed a three component model. However, by sequentially coupling the components we can limit the analysis to the two component case. For example, we can first couple the free-free holder and tool to form the substructure I-II identified in Fig. 7.6.2. To carry out this step, we begin by defining the components and coordinates as

[11] Author T. Schmitz recognizes the significant contributions of G.S. Duncan, Valparaiso University, to this section.

[12] US Patent application 20070088456.

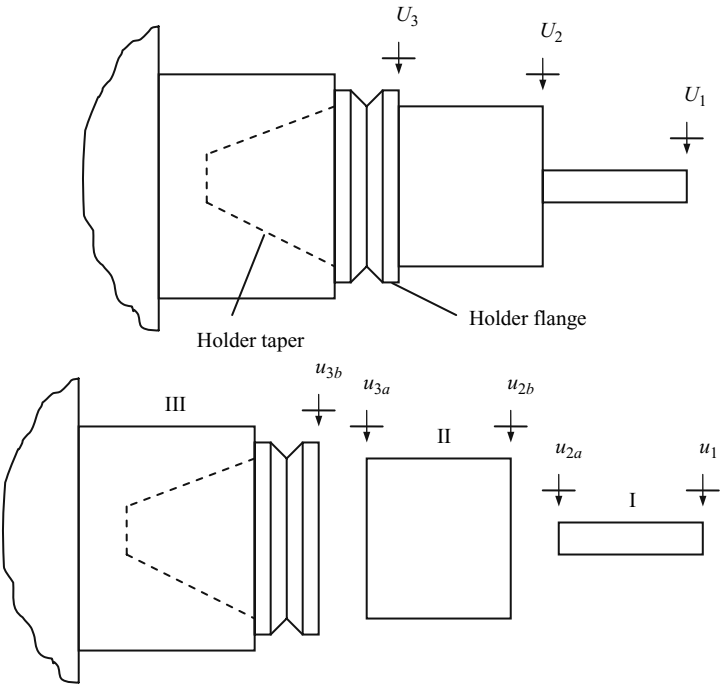

Fig. 7.6.1 Three component receptance coupling model of tool (I), holder (II), and spindle-machine (III)

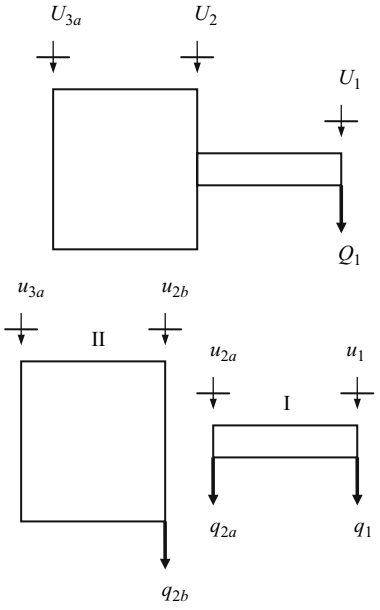

Fig. 7.6.2 (Sub)assembly I-II composed of tool (I) and holder (II). The generalized force Q_1 is applied to U_1 to determine G_{11} and G_{3a1}

displayed in Fig. 7.6.2. We then calculate the component receptances. If we apply the Euler-Bernoulli receptances described by Bishop and Johnson [1], the appropriate equations are provided in Table 7.4.2. For I, we have the free-free receptances: $h_{11} = \frac{-c_1}{\lambda^3 c_7}$, $l_{11} = n_{11} = \frac{c_2}{\lambda^2 c_7}$, $p_{11} = \frac{c_5}{\lambda c_7}$, $h_{2a2a} = \frac{-c_1}{\lambda^3 c_7}$, $l_{2a2a} = n_{2a2a} = \frac{-c_2}{\lambda^2 c_7}$, $p_{2a2a} = \frac{c_5}{\lambda c_7}$, $h_{12a} = h_{2a1} = \frac{c_3}{\lambda^3 c_7}$, $l_{12a} = n_{2a1} = \frac{-c_4}{\lambda^2 c_7}$, $l_{2a1} = n_{12a} = \frac{c_4}{\lambda^2 c_7}$, and $p_{12a} = p_{2a1} = \frac{c_6}{\lambda c_7}$, where $\lambda^4 = \omega^2 \frac{\rho A}{EI(1+i\eta)}$, and L, ρ, A, E, I, and η depend on the tool geometry and material properties. For II, we simply replace coordinate 1 with $2b$ and coordinate $2a$ with $3a$ in the previous equations. Additionally, we must use the holder geometry and material properties to define λ, L, ρ, A, E, I, and η. We will assume a rigid coupling between these two components and follow the approaches described previously to determine the I-II (sub)assembly tip receptances: (direct) G_{11} and G_{3a3a}; and (cross) G_{13a} and G_{3a1}.

To find G_{11} and G_{3a1}, we apply Q_1 to coordinate U_1 as shown in Fig. 7.6.2. The components' displacements/rotations are: $u_1 = R_{11}q_1 + R_{12a}q_{2a}$, $u_{2a} = R_{2a1}q_1 + R_{2a2a}q_{2a}$, $u_{2b} = R_{2b2b}q_{2b}$, and $u_{3a} = R_{3a2b}q_{2b}$. The equilibrium conditions are: $q_{2a} + q_{2b} = 0$ and $q_1 = Q_1$. We substitute the component displacements/rotations and equilibrium conditions into the compatibility condition, $u_{2b} - u_{2a} = 0$, to obtain the expression for q_{2b} shown in Eq. 7.6.1. The component force q_{2a} is then determined from the equilibrium condition $q_{2a} = -q_{2b}$. The expression for G_{11} is provided in Eq. 7.6.2. The cross receptance matrix G_{3a1} is shown in Eq. 7.6.3.

$$\begin{aligned} u_{2b} - u_{2a} &= 0 \\ R_{2b2b}q_{2b} - R_{2a1}q_1 - R_{2a2a}q_{2a} &= 0 \\ (R_{2a2a} + R_{2b2b})q_{2b} - R_{2a1}Q_1 &= 0 \\ q_{2b} &= (R_{2a2a} + R_{2b2b})^{-1}R_{2a1}Q_1 \end{aligned} \tag{7.6.1}$$

$$G_{11} = \frac{U_1}{Q_1} = \frac{u_1}{Q_1} = \frac{R_{11}q_1 + R_{12a}q_{2a}}{Q_1} = \frac{R_{11}Q_1 - R_{12a}(R_{2a2a} + R_{2b2b})^{-1}R_{2a1}Q_1}{Q_1}$$

$$G_{11} = R_{11} - R_{12a}(R_{2a2a} + R_{2b2b})^{-1}R_{2a1} = \begin{bmatrix} H_{11} & L_{11} \\ N_{11} & P_{11} \end{bmatrix} \tag{7.6.2}$$

$$G_{3a1} = \frac{U_{3a}}{Q_1} = \frac{u_{3a}}{Q_1} = \frac{R_{3a2b}q_{2b}}{Q_1} = \frac{R_{3a2b}(R_{2a2a} + R_{2b2b})^{-1}R_{2a1}Q_1}{Q_1}$$

$$G_{3a1} = R_{3a2b}(R_{2a2a} + R_{2b2b})^{-1}R_{2a1} = \begin{bmatrix} H_{3a1} & L_{3a1} \\ N_{3a1} & P_{3a1} \end{bmatrix} \tag{7.6.3}$$

We find the remaining tip receptances G_{3a3a} and G_{13a} by applying Q_{3a} to coordinate U_{3a} as shown in Fig. 7.6.3. The components displacements/rotations are: $u_1 = R_{12a}q_{2a}$, $u_{2a} = R_{2a2a}q_{2a}$, $u_{2b} = R_{2b2b}q_{2b} + R_{2b3a}q_{3a}$, and $u_{3a} = R_{3a2b}q_{2b} + R_{3a3a}q_{3a}$. The equilibrium conditions are: $q_{2a} + q_{2b} = 0$ and $q_{3a} = Q_{3a}$. In the same manner as before, we substitute the component displacements/rotations and equilibrium conditions into the compatibility condition, $u_{2a} - u_{2b} = 0$, to determine q_{2a}; see Eq. 7.6.4. The component force q_{2b} is found

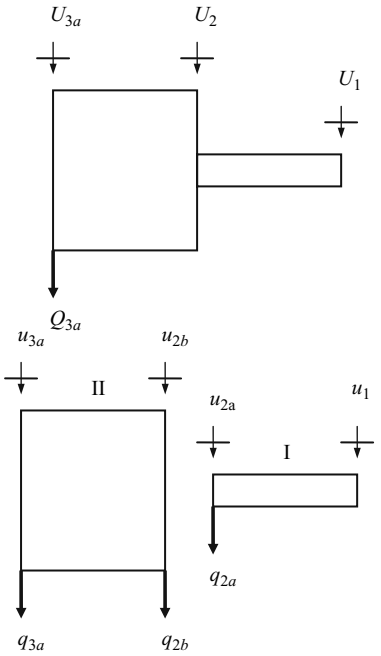

Fig. 7.6.3 (Sub)assembly I-II composed of tool (I) and holder (II). The generalized force Q_{3a} is applied to U_{3a} to determine G_{3a3a} and G_{13a}

from $q_{2b} = -q_{2a}$. The equation for the direct receptance G_{3a3a} is shown in Eq. 7.6.5, while the cross receptance G_{13a} is provided in Eq. 7.6.6.

$$\begin{aligned} u_{2a} - u_{2b} &= 0 \\ R_{2a2a}q_{2a} - R_{2b2b}q_{2b} - R_{2b3a}q_{3a} &= 0 \\ (R_{2a2a} + R_{2b2b})q_{2a} - R_{2b3a}Q_{3a} &= 0 \\ q_{2a} &= (R_{2a2a} + R_{2b2b})^{-1}R_{2b3a}Q_{3a} \end{aligned} \tag{7.6.4}$$

$$G_{3a3a} = \frac{U_{3a}}{Q_{3a}} = \frac{u_{3a}}{Q_{3a}} = \frac{R_{3a3a}q_{3a} + R_{3a2b}q_{2b}}{Q_{3a}} = \frac{R_{3a3a}Q_{3a} - R_{3a2b}(R_{2a2a} + R_{2b2b})^{-1}R_{2b3a}Q_{3a}}{Q_{3a}}$$

$$G_{3a3a} = R_{3a3a} - R_{3a2b}(R_{2a2a} + R_{2b2b})^{-1}R_{2b3a} = \begin{bmatrix} H_{3a3a} & L_{3a3a} \\ N_{3a3a} & P_{3a3a} \end{bmatrix} \tag{7.6.5}$$

$$G_{13a} = \frac{U_1}{Q_{3a}} = \frac{u_1}{Q_{3a}} = \frac{R_{12a}q_{2a}}{Q_{3a}} = \frac{R_{12a}(R_{2a2a} + R_{2b2b})^{-1}R_{2b3a}Q_{3a}}{Q_{3a}}$$

$$G_{13a} = R_{12a}(R_{2a2a} + R_{2b2b})^{-1}R_{2b3a} = \begin{bmatrix} H_{13a} & L_{13a} \\ N_{13a} & P_{13a} \end{bmatrix} \tag{7.6.6}$$

Now that we've coupled components I and II to form the (sub)assembly I-II, we can rigidly couple this result to the spindle-machine. See Fig. 7.6.4, which is

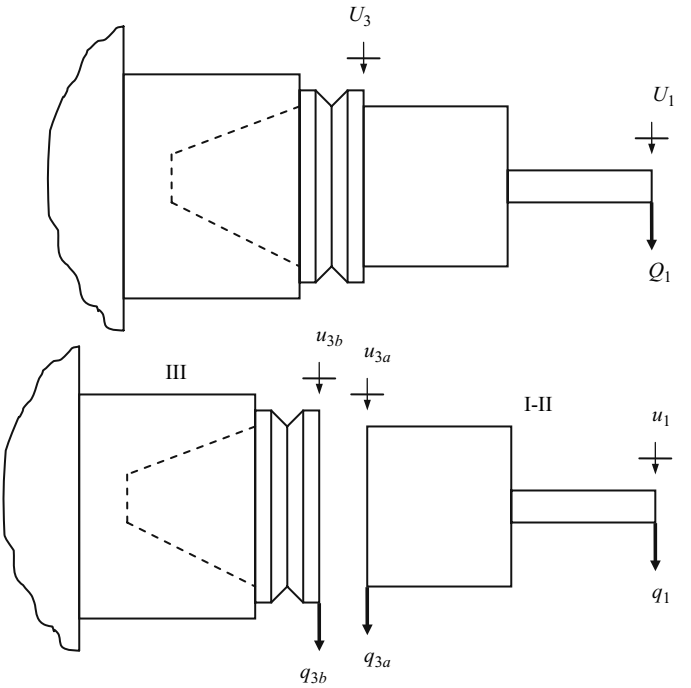

Fig. 7.6.4 The I-II (sub)assembly is rigidly coupled to the spindle-machine (III) to determine the tool point receptances, G_{11}

very similar to Fig. 7.3.3. To apply Eq. 7.3.13, we must make minor modifications to the subscripts to match our new coordinates. Relative to the original equation, we see that we must replace coordinate $2a$ with $3a$ and coordinate $2b$ with $3b$. Therefore, the tool point receptances are defined by:

$$G_{11} = R_{11} - R_{13a}(R_{3a3a} + R_{3b3b})^{-1} R_{3a1}, \tag{7.6.7}$$

where the R_{ij} matrices are the (sub)assembly matrices from the I-II coupling result. Therefore, we have: $R_{11} = G_{11}$ from Eq. 7.6.2, $R_{3a1} = G_{3a1}$ from Eq. 7.6.3, $R_{3a3a} = G_{3a3a}$ from Eq. 7.6.5, and $R_{13a} = G_{13a}$ from Eq. 7.6.6. We still have one matrix in Eq. 7.6.7 that is unknown, however. We do yet not know the spindle-machine receptances R_{3b3b}.

7.6.1 Spindle-Machine Receptances

Before discussing R_{3b3b} in more detail, let's take another look at the model in Fig. 7.6.1. We notice that the section of the tool holder beyond the

flange has been artificially separated from the rest of the holder, which includes the portion that is inserted and clamped in the spindle. There are two reasons for this approach. First, for a given spindle, all holders inserted in that spindle will typically have the same flange geometry. In general, it is only the portion of the holder beyond the flange that varies from one holder to the next; this is necessary for automatic tool changes. Second, the portion of the spindle that we need to excite and measure is the spindle shaft itself. Unfortunately, typical spindle designs do not give us access to the spindle shaft. It is located within the spindle housing and interfaces with the holder-spindle coupling mechanism (such as HSK, CAT, or other). Therefore, it is convenient to consider the holder flange and taper to be part of the spindle itself. This also locates potential flexibility in the holder-spindle coupling within the measured spindle receptances so that they do not have to be separately modeled.

Given our discussion of impact testing in Section 2.6, we see that the direct FRF h_{3b3b} would be straightforward to obtain. We'd simply need to modify a holder to remove the portion beyond the flange, place this artifact in the spindle, and then excite spindle-machine at the free end of the holder (on the flange), while measuring the response at the same location. However, as we've discussed, we also require the direct displacement-to-couple, rotation-to-force, and rotation-to-couple FRFs to fully populate the R_{3b3b} matrix. These additional receptances are not so easy to obtain experimentally. Exciting the system with an impulsive couple is particularly challenging. Therefore, we can consider a different approach.

Rather than using a measurement artifact that includes only the flange and taper, let's select an artifact that incorporates some length beyond the flange as shown in Fig. 7.6.5. If we can determine the assembly matrix $G_{22} = \begin{bmatrix} H_{22} & L_{22} \\ N_{22} & P_{22} \end{bmatrix}$ experimentally, then we can use this information, together with a model of the portion of the artifact beyond the flange, to determine R_{3b3b}. By replacing coordinate 1 with 2, coordinate $2a$ with $3a$, and coordinate $2b$ with $3b$ in Eq. 7.3.13, we obtain the free end response for the artifact-spindle-machine assembly:

$$G_{22} = R_{22} - R_{23a}(R_{3a3a} + R_{3b3b})^{-1} R_{3a2}. \tag{7.6.8}$$

We can rearrange Eq. 7.6.8 to isolate R_{3b3b}. See Eq. 7.6.9, where the R_{ij} matrices are obtained from a model of the free-free portion of the artifact beyond the flange (component II in Fig. 7.6.5) and G_{22} is determined from measurements. We can describe this decomposition process of identifying the substructure receptances, R_{3b3b}, from the measured assembly receptances, G_{22}, and modeled substructure receptances, R_{3a2}, R_{22}, R_{23a} , and R_{3a3a}, as "inverse RCSA".

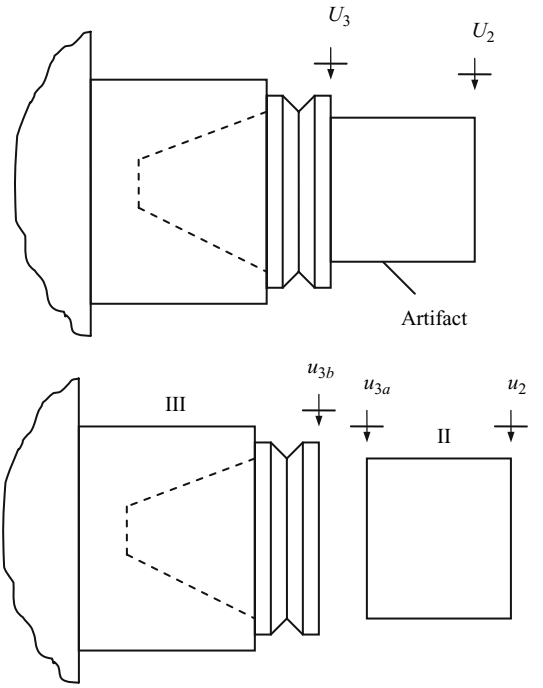

Fig. 7.6.5 Artifact model for G_{22} measurement; these receptances are subsequently used to determine R_{3b3b} by inverse RCSA (Eq. 7.6.9)

$$\begin{aligned} G_{22} - R_{22} &= -R_{23a}(R_{3a3a} + R_{3b3b})^{-1} R_{3a2} \\ R_{23a}^{-1}(R_{22} - G_{22})R_{3a2}^{-1} &= (R_{3a3a} + R_{3b3b})^{-1} \\ R_{3a2}(R_{22} - G_{22})^{-1} R_{23a} &= R_{3a3a} + R_{3b3b} \\ R_{3b3b} &= R_{3a2}(R_{22} - G_{22})^{-1} R_{23a} - R_{3a3a} \end{aligned} \tag{7.6.9}$$

Our only remaining task is to define the G_{22} receptances. The displacement-to-force term $H_{22} = \frac{X_2}{F_2}$ is straightforward to obtain. We simply excite the assembly at coordinate 2, typically via an impact hammer, and record the response at the same location using, for example, an accelerometer, laser vibrometer, or capacitance probe. To find the rotation-to-force receptance $N_{22} = \frac{\Theta_2}{F_2}$, we can implement a first order finite difference approach [27]. By measuring both the direct FRF H_{22} and cross FRF $H_{2a2} = \frac{X_{2a}}{F_2}$, we can compute N_{22} according to Eq. 7.6.10. The displacement-to-force cross FRF H_{2a2} is obtained by exciting the assembly at U_2 and measuring the response at coordinate U_{2a}, located a distance S from the artifact's free end, as shown in Fig. 7.6.6.

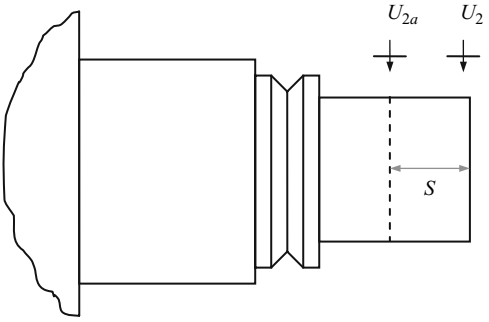

Fig. 7.6.6 Locations for direct and cross artifact-spindle-machine assembly measurements

Equivalently, we could measure H_{22a}, where the linear transducer is placed at U_2 and the force is applied at U_{2a}.

$$N_{22} = \frac{H_{22} - H_{2a2}}{S} = \frac{H_{22} - H_{22a}}{S} \tag{7.6.10}$$

We can assume reciprocity to establish the equality: $L_{22} = N_{22}$. (We see this same behavior for the free-free beam receptances in Table 7.4.2.) We cannot rely on reciprocity or finite difference computations to find P_{22}. However, using the other three artifact-spindle-machine receptances, we can synthesize P_{22} [28]. See Eq. 7.6.11. Given P_{22}, we have now fully populated G_{22} and we can use Eq. 7.6.9 to obtain R_{3b3b}.

$$P_{22} = \frac{\Theta_2}{M_2} = \frac{F_2}{X_2}\frac{X_2}{M_2}\frac{\Theta_2}{F_2} = \frac{1}{H_{22}}L_{22}N_{22} = \frac{N_{22}^2}{H_{22}} \tag{7.6.11}$$

7.6.2 Summary

Let's conclude the chapter by summarizing the RCSA steps and discussing implementation considerations. Given the three component model shown in Fig. 7.6.1, our initial task is to identify the substructure receptances. We find the tool (I) and holder (II) free-free receptances from models. These may be based on Euler-Bernoulli beam theory or finite element computations, for example. We use artifact measurements and inverse RCSA to determine the spindle-machine (III) receptances. Once we have the substructure dynamics defined, we sequentially couple the three component receptance matrices to obtain the tool point FRF, H_{11}, that is required for the stability and surface location error analyses described in Chapters 4, 5, and 6. A benefit of this technique is that

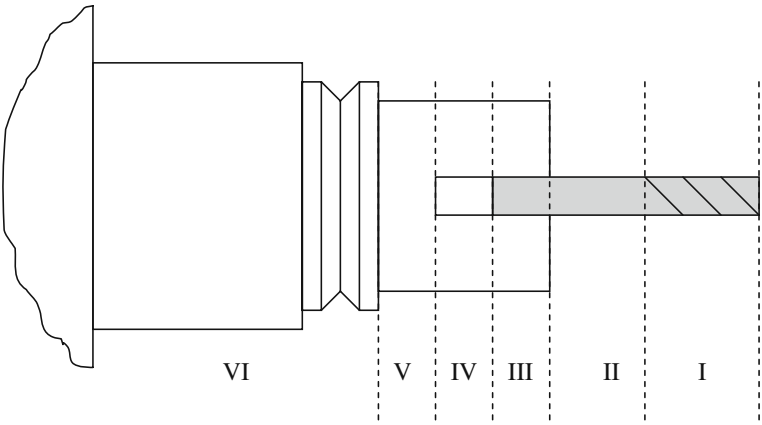

Fig. 7.6.7 Component definitions to account for changes in cross sectional dimensions and the portion of the tool inserted in the holder

once the spindle-machine receptances have been identified, any tool-holder combination can be coupled to the selected spindle without the need for additional measurements.

A final point for consideration is the tool and holder models. One issue is that a portion of the tool is inserted in the holder; see component III in Fig. 7.6.7. This gives the potential for cross sections with different material properties between a steel holder and carbide tool, for example. Equivalent structural rigidity, EI_{eq}, and mass per unit length, ρA_{eq}, values can be calculated as shown in Eqs. 7.6.12 and 7.6.13, where the h and t subscripts indicate the holder and tool, respectively. These may then be substituted for the EI and ρA products in the Euler-Bernoulli beam receptance equations defined in Table 7.4.2.

$$EI_{eq} = E_h I_h + E_t I_t \tag{7.6.12}$$

$$\rho A_{eq} = \rho_h A_h + \rho_t A_t \tag{7.6.13}$$

A second issue for the Euler-Bernoulli receptances is that constant cross sectional dimensions are required. Changes in cross section can be accommodated by defining a new component for each constant cross section portion. Components I through V are defined in Fig. 7.6.7 to represent the required tool and holder substructures. Here we see that a separate component, I, was defined for the fluted portion of the tool. This is necessary because the actual 2nd moment of area, I, and area, A, for the helical flutes differ from the cylindrical shank I and A values. One approach is to define an equivalent diameter that is then used in the I and A calculations. See [29, 30], for example.

IN A NUTSHELL If measurement of the tool tip FRF is convenient for the machine tool user, then the information required for pre-process predictions of machining performance can be directly obtained. However, if FRF measurements are difficult for the user to complete, then receptance coupling offers an alternative.

While receptance coupling requires accurate measurements of the spindle-machine substructure, these measurements certainly fall within the domain of expert consultants. If the spindle-machine response is archived and the computations are embedded in software, then the power of a machine tool user to predict the assembly FRF for a new unmeasured tool is formidable. The predicted FRF can be used to compute stability lobes and surface location error and enable the end user significant advantage because he/she will know which cuts are acceptable and which are not for the selected tool-holder-spindle-machine combination.

The previous scenario highlights the thrust of this book. It is possible to use the techniques described here to predict machining performance with sufficient accuracy that the trial and error process development approach so prevalent in machining operations today can be rendered obsolete.

Exercises

1. Determine the direct frequency response function, $\frac{X_2}{F_2}$, for the two degree of freedom system shown in Fig. e.7.1 using receptance coupling. Express your final result as a function of m, c, k, and the excitation frequency, ω. You may assume a harmonic forcing function, F_2, is applied to coordinate X_2.

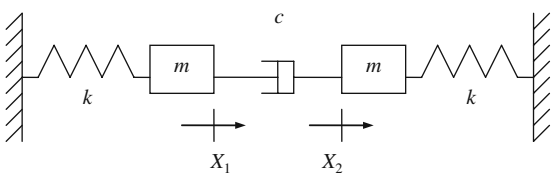

Fig. e.7.1 Two degree of freedom assembly

2. Determine the direct frequency response function, $\frac{X_1}{F_1}$, for the two degree of freedom system shown in Fig. e.7.2 using receptance coupling. Express your final result as a function of m, c, k, and the excitation frequency, ω. You may assume a harmonic forcing function, F_1, is applied to coordinate X_1.
3. Plot the displacement-to-force tip receptance for a sintered carbide cylinder with free-free boundary conditions. The beam is described by the following parameters: 19 mm diameter, 150 mm length, 550 GPa elastic modulus,

and 15000 kg/m^3 density. Assume a solid damping factor of 0.002. Select a frequency range that encompasses the first three bending modes and display your results as magnitude (m/N) vs. frequency (Hz) in a semilog format.

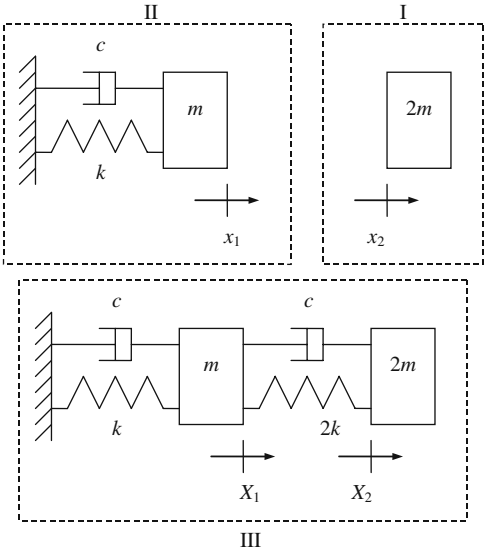

Fig. e.7.2 Flexible damped coupling of mass (I) to spring-mass-damper (II) to form the two degree of freedom assembly (III)

4. Use receptance coupling to rigidly join two free-free beams and find the free-free assembly's displacement-to-force tip receptance. Both steel cylinders are described by the following parameters: 12.7 mm diameter, 100 mm length, 200 GPa elastic modulus, and 7800 kg/m^3 density. Assume a solid damping factor of 0.0015. Once you have determined the assembly response, verify your result against the displacement-to-force tip receptance for a 12.7 mm diameter, 200 mm long free-free steel cylinder with the same material properties. Select a frequency range that encompasses the first three bending modes and display your results as the real (m/N) and imaginary (m/N) parts vs. frequency (Hz) using a linear scale.

References

1. Bishop, R. and Johnson, D., 1960, The Mechanics of Vibration, Cambridge University Press, Cambridge.
2. Jetmundsen, B., Bielawa, R., and Flannelly, W., 1988, Generalized Frequency-Domain Substructure Synthesis, Journal of the American Helicopter Society, 33: 55–64.
3. Schmitz, T. and Donaldson, R., 2000, Predicting High-Speed Machining Dynamics by Substructure Analysis, Annals of the CIRP, 49/1: 303–308.

4. Schmitz, T., Davies, M., and Kennedy, M., 2001, Tool Point Frequency Response Prediction for High-Speed Machining by RCSA, Journal of Manufacturing Science and Engineering, 123: 700–707.
5. Schmitz, T., Davies, M., Medicus, K., and Snyder, J., 2001, Improving High-Speed Machining Material Removal Rates by Rapid Dynamic Analysis, Annals of the CIRP, 50/1: 263–268.
6. Burns, T., Schmitz, T., 2004, Receptance Coupling Study of Tool-Length Dependent Dynamic Absorber Effect, Proceedings of American Society of Mechanical Engineers International Mechanical Engineering Congress and Exposition, IMECE2004-60081, Anaheim, CA.
7. Schmitz, T., and Duncan, G.S., 2005, Three-Component Receptance Coupling Substructure Analysis for Tool Point Dynamics Prediction, Journal of Manufacturing Science and Engineering, 127/4: 781–790.
8. Duncan, G.S., Tummond, M., and Schmitz, T., 2005, An Investigation of the Dynamic Absorber Effect in High-Speed Machining, International Journal of Machine Tools and Manufacture, 45: 497–507.
9. Cheng, C.-H., Schmitz, T., Arakere, N., and Duncan, G.S., 2005, An Approach for Micro End mill Frequency Response Predictions, Proceedings of American Society of Mechanical Engineers International Mechanical Engineering Congress and Exposition, IMECE2005-81215, Orlando, FL.
10. Burns, T. and Schmitz, T., 2005, A Study of Linear Joint and Tool Models in Spindle-Holder-Tool Receptance Coupling, Proceedings of 2005 American Society of Mechanical Engineers International Design Engineering Technical Conferences and Computers and Information in Engineering Conference, DETC2005-85275, Long Beach, CA.
11. Schmitz, T., Powell, K., Won, D., Duncan, G.S., Sawyer, W.G., Ziegert, J., 2007, Shrink Fit Tool Holder Connection Stiffness/Damping Modeling for Frequency Response Prediction in Milling, International Journal of Machine Tools and Manufacture, 47/9: 1368–1380.
12. Cheng, C.-H., Duncan, G.S., and Schmitz, T., 2007, Rotating Tool Point Frequency Response Prediction using RCSA, Machining Science and Technology, 11/3: 433–446.
13. Ewins, D., 1986, Analysis of Modified or Coupled Structures using FRF Properties, Report No. 86002, Imperial College London, Dynamics Section, Mechanical Engineering, London, England.
14. Ferreira, J. and Ewins, D., 1995, Nonlinear Receptance Coupling Approach Based on Describing Functions, Proceedings of the 14th International Modal Analysis Conference, Dearborn, MI, 1034–1040.
15. Lui, W. and Ewins, D., 2002, Substructure Synthesis via Elastic Media, Journal of Sound and Vibration, 257/2: 361-379.
16. Schmitz, T., Davies, M., and Kennedy, M., 2000, High-Speed Machining Frequency Response Prediction for Process Optimization, Proceedings of the 2nd International Seminar on Improving Machine Tool Performance, La Baule, France.
17. Park, S., Altintas, Y., and Movahhedy, M., 2003, Receptance Coupling for End Mills, International Journal of Machine Tools and Manufacture, 43: 889–896.
18. Thomson, W. and Dahleh, M., 1998, Theory of Vibration with Application, 5th Ed., Prentice Hall, Upper Saddle River, NJ, Section 9.5.
19. Chapra, S. and Canale, R., 1985, Numerical Methods for Engineers with Personal Computer Applications, McGraw-Hill, Inc., New York, NY, Section 7.1.
20. Thomson, W. and Dahleh, M., 1998, Theory of Vibration with Application, 5th Ed., Prentice Hall, Upper Saddle River, NJ, Section 3.9.
21. Beards, C., 1996, Structural Vibration: Analysis and Damping, Arnold, London, Section 2.2.5.
22. Weaver, W., Jr., Timoshenko, S., and Young, D., 1990, Vibration Problems in Engineering, 5th Ed., John Wiley and Sons, New York, NY, Section 5.12.

23. Hutchinson, J., 2001, Shear Coefficients for Timoshenko Beam Theory, Journal of Applied Mechanics, 68: 87–92.
24. Schmitz, T., and Duncan, G.S., 2005, Three-Component Receptance Coupling Substructure Analysis for Tool Point Dynamics Prediction, Journal of Manufacturing Science and Engineering, 127/4: 781-790, Appendix A: Beam Receptance Modeling.
25. Tlusty, J., Smith, S., and Winfough, W.R., 1996, Techniques for the Use of Long Slender End Mills in High-speed Milling, Annals of the CIRP, 45/1: 393–396.
26. Davies, M., Dutterer, B., Pratt, J., and Schaut, A., 1998, On the Dynamics of High-Speed Milling with Long, Slender Endmills, Annals of the CIRP, 47/1: 55–60.
27. Sattinger, S., 1980, A Method for Experimentally Determining Rotational Mobilities of Structures, Shock and Vibration Bulletin, 50: 17–27.
28. Ewins, D., 2000, Modal Testing: Theory, Practice and Application, 2nd Ed., Research Studies Press, Philadelphia, PA.
29. Kops, L. and Vo, D., 1990, Determination of the Equivalent Diameter of an End Mill Based on its Compliance, Annals of the CIRP, 39/1: 93–96.
30. Kivanc, E. and Budak, E., 2004, Structural Modeling of End Mills for Form Error and Stability Analysis, International Journal of Machine Tools and Manufacture, 44: 1151–1161.